CO_2 Capture by Absorption with Potassium Carbonate
Fourth Quarterly Report 2006

Quarterly Progress Report
Reporting Period Start Date: October 1, 2006
Reporting Period End Date: December 31, 2006

Authors: Gary T. Rochelle, Eric Chen, Babatunde Oyenekan,
Andrew Sexton, Jason Davis, Marcus Hilliard, Qing Xu, David Van Wagener, Jorge M. Plaza,
Amornvadee Veawab (University of Regina), Manjula Nainar (University of Regina)

January 27, 2007
DOE Award #: DE-FC26-02NT41440
Department of Chemical Engineering
The University of Texas at Austin

Disclaimer

Abstract

The objective of this work is to improve the process for CO_2 capture by alkanolamine absorption/stripping by developing an alternative solvent, aqueous K_2CO_3 promoted by piperazine. The best solvent and process configuration, matrix with MDEA/PZ, offers 22% and 15% energy savings over the baseline and improved baseline, respectively, with stripping and compression to 10 MPa. The energy requirement for stripping and compression to 10 MPa is about 20% of the power output from a 500 MW power plant with 90% CO_2 removal. The stripper rate model shows that a 'short and fat' stripper requires 7 to 15% less equivalent work than a 'tall and skinny' one. The stripper model was validated with data obtained from pilot plant experiments at the University of Texas with 5m K^+/2.5m PZ and 6.4m K^+/1.6m PZ under normal pressure and vacuum conditions using Flexipac AQ Style 20 structured packing. Experiments with oxidative degradation at low gas rates confirm the effects of Cu^{+2} catalysis; in MEA/PZ solutions more formate and acetate is produced in the presence of Cu^{+2}. At 150^{o}C, the half life of 30% MEA with 0.4 moles CO_2/mole amine is about 2 weeks. At 100^{o}C, less than 3% degradation occurred in two weeks. The solubility of potassium sulfate in MEA solution increases significantly with CO_2 loading and decreases with MEA concentration. The base case corrosion rate in 5 M MEA/1,2M PZ is 22 mpy. With 1 wt% heat stable salt, the corrosion rate increases by 50% to 160% in the order: thiosulfate< oxalate<acetate<formate. Cupric carbonate is ineffective in the absence of oxygen, but 50 to 250 ppm reduces corrosion to less than 2 mpy in the presence of oxygen.

Contents

List of Figures

List of Tables

Introduction

The objective of this work is to improve the process for CO_2 capture by alkanolamine absorption/stripping by developing an alternative solvent, aqueous K_2CO_3 promoted by piperazine. This work expands on parallel bench-scale work with system modeling and pilot plant measurements to demonstrate and quantify the solvent process concepts.

Gary Rochelle is supervising the bench-scale and modeling work. Three graduate students (Eric Chen, Babatunde Oyenekan, and Andrew Sexton) have received support during this quarter for direct effort on the scope of this contract. Five students supported by other funding have made contributions this quarter to the scope of this project (Marcus Hilliard, Jason Davis, Jorge Plaza, David Van Wagener, Qing Xu – Industrial Associates Program). Subcontract work was performed by Manjula Nainar at the University of Regina under the supervision of Amy Veawab.

Experimental

Subtasks 1.3a and 1.9b describe development of a model in RateSep™ for the absorber.

Subtask 1.9a describes further development of a rate model in ACM for the stripper.

Subtask 3.1 presents methods for analyzing amine degradation products by anion and cation chromatography. It describes two methods for preparing samples of degraded solutions.

Subtask 3.3 describes a method of gas chromatography for amine degradation products.

Subtask 3.4 describes methods to use the high temperature gas FTIR to determine amine and CO_2 vapor pressure over loaded solutions of piperazine.

Subtask 4.1 describes a method for measuring the solubility of potassium sulfate in loaded amine solutions with ion conductivity.

Task 5 describes electrochemical methods for measuring corrosion.

Results and Discussion

Progress has been made on five subtasks in this quarter:

Subtask 1.3a – Absorber Model

The RateSep model of the Absorber has been corrected to represent HPZCOO ion as a molecule while predicting an accurate heat of CO_2 absorption. The concentration-based kinetics of Cullinane have been converted to activity-based kinetics for input to RateSep™.

Subtask 1.3b – Stripper model

The rate-based model has been used to estimate the packing height for simple strippers at normal pressure and vacuum. This work has been reported in a PhD dissertation that will be submitted as a DOE topical report.

Subtask 1.8a – Predict Flowsheet Options

The equilibrium model has been used to evaluate energy requirements with a number of stripper configurations and solvent compositions. This work has been reported in a PhD dissertation that will be submitted as a DOE topical report.

Subtask 1.9 – Economic Analysis

Parameters and equations have been developed to present the 4.5 m K^+/4.5 m PZ solvent in the rate-based models for the absorber and stripper.

Subtask 3.1 – Analysis of Degradation Products

Additional degradation experiments have been performed with 2.5 m PZ/5 m $KHCO_3$ (with V) and 2.5 m PZ (with V and inhibitor A). Analyses have been completed on earlier experiments with MEA (5 ppm Fe) and MEA/PZ (5 ppm Fe, 250 ppm Cu).

Subtask 3.3 – Thermal Degradation

Samples of loaded MEA were degraded at 150°C and 100°C. These initial samples were analyzed by gas chromatography.

Subtask 3.4 – Amine Volatility

CO_2 and piperazine vapor pressure have been determined over loaded solutions of 2 m piperazine.

Subtask 4.1 – Sulfate Precipitation

The solubility of potassium sulfate was measured in solutions of MEA and MEA/PZ.

Subtask 5.1 – Corrosion in base solution compared to MEA

Electrochemical measurements of corrosion have been performed in solutions of 5M MEA/1.2 piperazine at 80°C with 0.2 mol CO2/mol amine.

Conclusions

1. The HPZCOO species can be correctly represented as a molecule in the RateSep™ model when appropriate values are entered for the heat of formation, heat capacity parameters, and heat of vaporization.

2. The best solvent and process configuration, matrix with MDEA/PZ, offers 22% and 15% energy savings over the baseline and improved baseline, respectively, with stripping and compression to 10 MPa. The energy requirement for stripping and compression to 10 MPa is about 20% of the power output from a 500 MW power plant with 90% CO_2 removal.

3. The stripper rate model shows that a 'short and fat' stripper requires 7 to 15% less equivalent work than a 'tall and skinny' one. The optimum stripper design could be one that operates between 50% and 80% flood at the bottom. Stripping at 30 kPa and 160 kPa requires 230 s and 115 s of effective packing volume to get an equivalent work 4% greater than the minimum.

5. The stripper model was validated with data obtained from pilot plant experiments at the University of Texas with 5m K^+/2.5m PZ and 6.4m K^+/1.6m PZ under normal pressure and vacuum conditions using Flexipac AQ Style 20 structured packing. Foaming was experienced during tests. The effective packing height in the stripper was 5.09m for 5m K^+/2.5m PZ and 6.47m for 6.4m K^+/1.6m PZ, but with a major derating of wetted area in the top half of the stripper.

6. The Cullinane model for VLE and rates at stripper conditions in 4.5 m K^+/4.5 m PZ does not give reliable results at lower CO_2 loading.

7. Adjustments in the thermodynamic parameters for AspenPlus® are able to match within 2 to 4% the heat of absorption calculated by a flash calculation with that calculated by the Van Hoff equation.

8. Experiments with oxidative degradation at low gas rates confirm the effects of Cu^{+2} catalysis; in MEA/PZ solutions more formate and acetate is produced in the presence of Cu^{+2}.

9. Reproducible analysis of MEA has been achieved by gas chromatography using the HP-5 nonpolar column.

10. At 150°C, the half life of 30% MEA with 0.4 moles CO_2/mole amine is about 2 weeks. At 100°C, less than 3% degradation occurred in two weeks.

11. The use of the FTIR apparatus for CO_2 solubility has been validated by measurements with loaded piperazine. The measured values of CO_2 vapor pressure agree well with values measured by Ermatchkov et al. (2006) and predicted by Hilliard (2005) at 40, 60, and 80 °C.

12. The solubility of potassium sulfate in MEA solution increases significantly with CO_2 loading and decreases with MEA concentration.

13. The base case corrosion rate in 5 M MEA/1,2M PZ is 22 mpy. With 1 wt% heat stable salt, the corrosion rate increases by 50% to 160% in the order: thiosulfate< oxalate<acetate<formate. Cupric carbonate is ineffective in the absence of oxygen, but 50 to 250 ppm reduces corrosion to less than 2 mpy in the presence of oxygen.

Future Work

We expect the following accomplishments in the next quarter:

Subtask 1.7 – Simulate and Optimize Packing Effects

The absorber data from campaigns 1, 2, and 4 will be simulated with the RateSep™ model.

Subtask 1.8a – Alternative Stripper Configurations

The PhD dissertation on this topic will be issued as a DOE topical report.

Subtask 1.9 – Economic Analysis

Heat and material balances will be developed for 4.5 m K^+/4.5 m PZ with the double matrix stripper configuration.

Subtask 3.1 – Analysis of Degradation Products

An experiment will be analyzed to quantify the effects of inhibitor A on piperazine oxidation.

Cation chromatography will used to determine the extent of piperazine degradation in the oxidation of MEA/PZ solution.

One additional unknown peak from ion chromatography will be identified.

Work will start on the development of a HPLC method for thermal degradation products of MEA and PZ.

Subtask 3.3 – Thermal Degradation

Samples of loaded MEA and potassium carbonate/PZ will be degraded at 100ºC and 150°C.

A method of analysis will be tested on an HPLC.

Subtask 3.4 – Amine Volatility

Measurements of CO_2 and amine vapor pressure will be completed for MEA, MEA/PZ, and PZ systems at 40 and 60°C.

Subtask 4.1 – Sulfate Precipitation

Additional measurements will be made of solubility of potassium sulfate solids in MEA solutions.

Subtask 5.4 – Effects of corrosion inhibitors

Corrosion of MEA/PZ solutions will be measured with the addition of Cu^{++} and inhibitor A.

Task 1 – Modeling Performance of Absorption/Stripping of CO2 with Aqueous K2CO3 Promoted by Piperazine

Subtask 1.3a – Absorber Model

by Eric Chen

(supported by this contract)

Introduction

The heats of absorption from the Aspen Plus® flash calculation were reconciled. The heat duty from the flash calculation was within ±4% of that calculated from the VLE data using the Van Hoff equation. The initial reconciliation was performed using a 0.0001 charge for the HPZCOO species, which slightly changed the VLE data and required a re-regression of the VLE parameters with the new charge. Attempts to re-regress the VLE parameters with the 0.0001 charge were unsuccessful and a different approach was undertaken.

In the Hilliard VLE regression analysis, the HPZCOO ion was treated as a molecule and not an ion (Hilliard 2005). Therefore, this treatment was adopted in order to maintain consistency. In the treatment of HPZCOO, the charge was set back to zero, and the heats of formation and heat capacity were treated as that of a molecule. After the heat of absorption and VLE were reconciled, the forward and reverse rate constants for the reactions of piperazine and CO_2 were inputted into the RateSep™ absorber model.

Experimental

Heat of Absorption Reconciliation

After unsuccessful attempts to re-regress the Hilliard VLE model with the 0.0001 charge for the HPZCOO species, it was decided to continue treating HPZCOO as a molecule. Therefore, the heat of formation for HPZCOO was inputted as DHFORM instead of DHAQFM. DHFORM represents the AspenPlus® input for the standard heat of formation of ideal gas at 298.15K. DHAQFM is the aqueous heat of formation at infinite dilution and is used in electrolyte solutions for ionic species and molecular solutes. The other piperazine species, PZH, PZCOO, and $PZ(COO)_2$ ions were treated as ions and the heats of formation were inputted as DHAQFM.

In addition, the heat capacity coefficients of HPZCOO were inputted into CPIG, which is the AspenPlus® worksheet used to enter the ideal gas heat capacity coefficients. The heat capacity coefficients for the PZH, PZCOO, and $PZ(COO)_2$ ions were inputted into the CPAQ0-1 tab, which contains the parameters for calculating aqueous phase heat capacity at infinite dilution. Finally, a zero enthalpy of vaporization was needed to "trick" AspenPlus® since the heat of formation and heat capacity parameter for HPZCOO were both inputted in the ideal gas state, but are actually in the liquid state. This was accomplished by inputting zeros into the parameter for the Watson Heat of Vaporization Correlation under the DHVLWT tab in AspenPlus®.

As expected, with the HPZCOO charge changed back to zero, a slight adjustment was made to each of the heats of formation and heat capacity parameters initially regressed. The updated parameters are shown below.

Table 1. Heats of Formation Used

Species	DHFORM kcal/mol	DHVLB kcal/mol	DHAQFM kcal/mol	$\Delta H_{f,298.15}$ Used kcal/mol	Source
$H_2O(l)$	-57.8	9.717	-	-68.315	DIPPR
H_3O^+	-	-	-68.269	-68.2693	Aspen
HCO_3^-	-	-	-165.279	-165.279	Aspen
PZ(l)	3.917	9.999	-	-5.39	Adjusted
PZH^+	-	-	-30.453	-	Calc
$PZCOO^-$	-	-	-123.307	-	Calc
$PZ(COO^-)_2$	-	-	-226.457	-	Calc
H^+PZCOO^-	-134.576	0	-	-	Calc

Table 2. Heat Capacity Constants for 2 Parameter Model

Species cal/mol-K	$C_P = A + BT$	
	A	B
H_2O	11.84	0.018
H_3O^+	17.98	
HCO_3^-	-7.44	0.066
PZ	19.33	0.089
PZH^+	164.05	0.071
PZCOO	172.97	0.137
$PZ(COO^-)_2$	226.74	0.184
H+PZCOO$^-$	179.11	0.118

Table 3 shows the results from the final heat of absorption reconciliation effort. From 298.15 to 343.15K (25 to 70°C), the heat of absorption from the two calculations are approximately ±3%. In the higher temperature ranges, from 373.15 to 393.15K, there is more deviation, with differences of ±6%.

Table 3. Reconciled Heats of Absorption Results

Temp K	P_{CO2} Pa	ΔH-HD kcal/mol	ΔH-VLE kcal/mol	Diff %
298.15	31.76	-20.39	-20.39	0.004
313.15	343.69	-17.19	-16.84	-2.07
333.15	24001	-11.18	-11.32	1.27
343.15	10677	-13.22	-12.85	-2.86
373.15	77922	-11.79	-11.99	1.66
383.15	50817	-10.22	-10.65	4.03
393.25	22704	-7.43	-7.86	5.56

Kinetics of Potassium Carbonate Promoted Piperazine

The kinetics for the absorption of carbon dioxide into aqueous potassium carbonate and piperazine were measured in a wetted wall column (Cullinane, 2005). Experiments were conducted with 0.45-3.6 m piperazine and 0-3.1 m potassium carbonate at 25-110°C. A rigorous kinetic model was developed and rate constants were regressed from the experimental data. The reaction of CO_2 with piperazine was modeled using the "zwitterion" mechanism. Carbon dioxide reacts with the amine to form a neutrally charged intermediate species, followed by the extraction of the proton by a base (Equations 1 and 2).

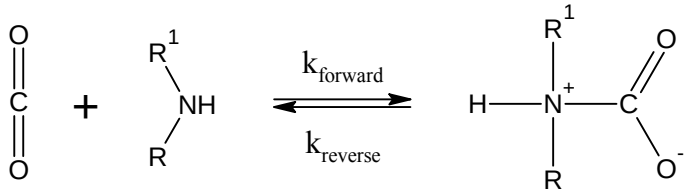

(1)

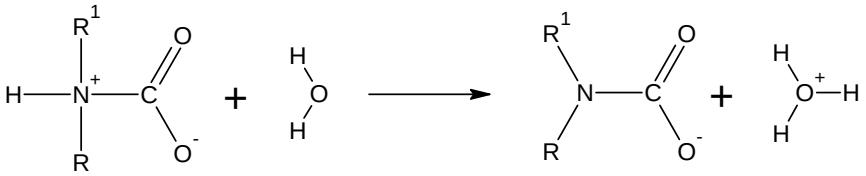

(2)

For the zwitterion mechanism, the rate of reaction can be written as:

$$r = \frac{[Am][CO_2]}{\frac{1}{k_f} + \frac{k_r}{k_f \sum_b k_{PZ-b}}} \tag{3}$$

If we assume that ∑kb[b] << kr, then the reaction can be re-written as:

$$rate_{CO_2} = \sum_b k_{Am-b}[Am][b][CO_2] \tag{4}$$

where:

$$k_{Am-b} = \frac{k_f k_b}{k_r} \tag{5}$$

The following amine reactions were used in the Cullinane model (2005):

$$PZ + CO_2 + \begin{cases} OH^- \xleftarrow{k_{PZ-OH^-}} PZCOO^- + H_2O \\ H_2O \xleftarrow{k_{PZ-H_2O}} PZCOO^- + H_3O \\ PZ \xleftarrow{k_{PZ-PZ}} PZCOO^- + PZH^+ \\ CO_3^{2-} \xleftarrow{k_{PZ-CO_3^{2-}}} PZCOO^- + HCO_3^- \\ PZCOO- \xleftarrow{k_{PZ-PZCOO^-}} PZCOO^- + H^+PZCOO^- \end{cases} \tag{6}$$

$$PZCOO^- + CO_2 + \begin{cases} H_2O \xleftarrow{k_{PZCOO^- - H_2O}} PZ(COO^-)_2 + H_3O \\ PZ \xleftarrow{k_{PZCOO^- - PZ}} PZ(COO^-)_2 + PZH^+ \\ CO_3^{2-} \xleftarrow{k_{PZCOO^- - CO_3^{2-}}} PZ(COO^-)_2 + HCO_3^- \\ PZCOO- \xleftarrow{k_{PZCOO^- - PZCOO^-}} PZ(COO^-)_2 + H^+PZCOO^- \end{cases} \quad (7)$$

According to Cullinane, hydroxide reactions were not included in the second set of reactions because the concentration is typically very small when $PZCOO^-$ is present. All of the buffering reactions were considered to be in equilibrium and reversible rate expressions for CO_2 with PZ and $PZCOO^-$ are given by the following:

$$r = \sum_b k_{PZ-b}[b]\left([PZ][CO_2] - \frac{K_w[PZCOO^-]}{K_{PZCOO^-}[OH^-]}\right) \quad (8)$$

$$r = \sum_b k_{PZCOO^- - b}[b]\left([PZCOO^-][CO_2] - \frac{K_w[PZ(COO^-)_2]}{K_{PZ(COO^-)_2}[OH^-]}\right) \quad (9)$$

The temperature dependence of the rate constants is given by the following:

$$k^\infty = k^o \exp\left(\frac{\Delta H_a}{R}\left(\frac{1}{T(K)} - \frac{1}{298.15}\right)\right) \quad (10)$$

where k^o is the rate constant at 298.15K and ΔH_a is the activation energy. An ionic strength correction is made to the rate constants by:

$$k = k^\infty \exp(0.3I) \quad (11)$$

where I is the ionic strength of the solution and given by the following:

$$I = \frac{1}{2}\sum_i \left(C_i z_i^2\right) \quad (12)$$

where C_i is the molar concentration and the z_i is the charge of the species i.

The catalysis of the formation of bicarbonate ion by hydroxide, piperazine, and piperazine carbamate was also included in the Cullinane model (2005). The reactions to form bicarbonate ion were included to properly model equilibrium in the boundary layer and do not affect the CO_2 absorption rate. The three reversible reactions are:

$$CO_2 + OH^- \xleftarrow{k_{OH^-}} HCO_3^- \quad (13)$$

$$PZ + CO_2 + H_2O \xleftarrow{k_{PZ}} PZH^+ + HCO_3^- \quad (14)$$

$$PZCOO^- + CO_2 + H_2O \xleftarrow{k_{PZCOO^-}} H^+PZCOO^- + HCO_3^- \quad (15)$$

The rate expression for bicarbonate formation is given by:

$$r = \sum_b k_b[b]\left([CO_2] - \frac{[HCO_3^-]}{K_{HCO_3^-}[OH^-]}\right) \quad (16)$$

The rate constant from Pohorecki (1988) for the reaction of CO_2 and OH^- was used. The reaction is dependent on ionic strength and is written as:

$$\log k_{OH^-} = \log k^{\infty}_{OH^-} + \sum_i \kappa_i I_i \tag{17}$$

where:

$$\log k^{\infty}_{OH^-} = 11.916 - \frac{2382.0}{T(K)} \tag{18}$$

and κ_i is the ion specific parameter and I_i is the ionic strength of species i.

The rates constants for bicarbonate formation by the amines were assumed to be the same as that determined for MDEA by Littel (1991) and is given by:

$$k_{Am}\left(\frac{m^3}{kmol \cdot s}\right) = 1.34 \times 10^9 \exp\left(\frac{-5771.0}{T(K)}\right) \tag{19}$$

The rate constant for the amine-catalyzed formation of bicarbonate was corrected for ionic strength using equation 11.

Conversion to Activity-Base Kinetics

In AspenPlus® 2006, the new version of RateSep™ allows the user to enter activities in terms of mole gamma using the power law kinetic expression:

$$r = k\left(\frac{T}{T_0}\right)^n \exp^{\left(\frac{-E}{R}\left(\frac{1}{T}-\frac{1}{T_0}\right)\right)} \prod (x_i \gamma_i)^{\alpha_i} \tag{20}$$

where k is the pre-exponential factor independent of temperature, n is the temperature exponent, E is the activation energy, T_0 is the reference temperature (298.15K), k is the pre-exponential factor, x_i is the reactant species i, γ_i is the activity coefficient, and α_i is the reaction order for the species. Since the equilibrium constants were already activity based, it made sense to implement activity based kinetics within the model as well.

The rate constants developed by Cullinane (2005) utilize concentration-based units and therefore needed to be converted into activity units. A simple algebraic manipulation was performed using the following equation:

$$k_a = \frac{k_c [PZ][CO_2][b]}{(x_{PZ}\gamma_{PZ})(x_{CO_2}\gamma_{CO_2})(x_b \gamma_b)(total\, mol/L)} \tag{21}$$

where k_a is the activity base rate constant, k_c is the concentration-based rate constant, [*i*] is the concentration of species *i* in units of mol/L, and x_i is the mole fraction and γ_i is the activity coefficient. The last term in the denominator represents the total molar concentration per liter of solvent and will be specific for a particular solvent composition and loading. Therefore, a representative total molar concentration was selected and assumed to be constant across the column.

The kinetics developed by Cullinane (2005) also contains a correction for ionic strength. However, in AspenPlus®, this correction cannot be directly implemented. Therefore, a representative ionic strength at 50C and 0.5 loading (mol CO_2/Total Alkalinity) was selected and assumed to be constant over the various temperature and loading ranges. Figure 1 shows that this assumption is valid over the various temperature and loading ranges.

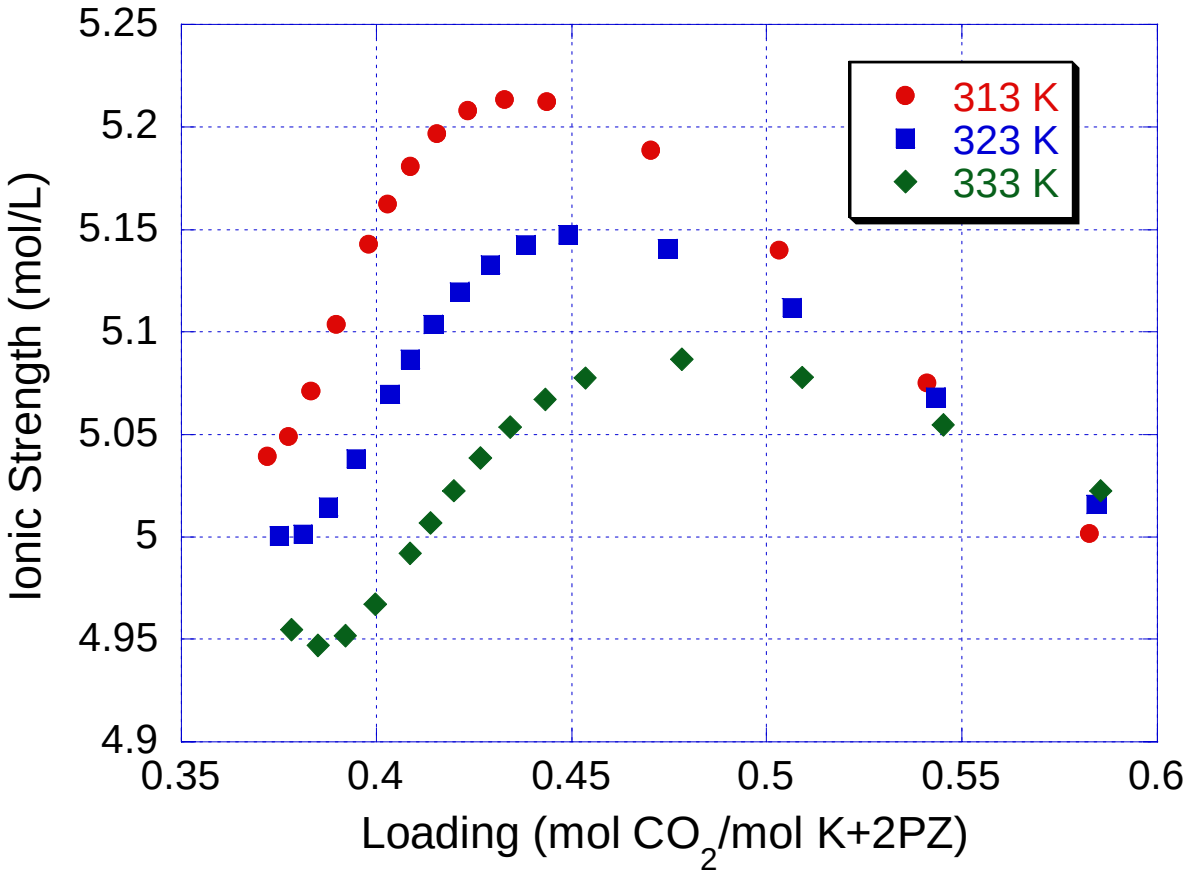

Figure 1. Ionic Strength of 5.0m K+/2.5m PZ solution generated by AspenPlus® from 313 to 333K

The overall rate for the reversible reactions is given by the difference between the forward and reverse rate and is given by the following equations:

$$rate = \sum_b k_{PZ-b}\left(a_{PZ}a_{CO_2}a_b - \frac{a_{PZCOO}a_{Hb}}{K_{PZ-b}}\right)$$
$$rate = \sum_b k_{PZCOO^--b}\left(a_{PZCOO^-}a_{CO_2}a_b - \frac{a_{PZ(COO^-)2}a_{Hb}}{K_{PZCOO^--b}}\right) \quad (22)$$

where $k_{PZ/PZCOO\text{-}b}$ is the forward rate constant in activity units, $K_{PZ/PZCOO\text{-}b}$ is the equilibrium constant, and a_i is the activity of the species ($x_i \cdot \gamma_i$).

Table 4. Forward 5mK$^+$/2.5mPZ Activity-Based Rate Parameters for Piperazine, Piperazine, and Bicarbonate Reaction as Inputted into AspenPlus® RateSep™

Eqn No.	Reaction	$Rate_{for} = k\left(\frac{T}{T_o}\right)^n \exp\left(\frac{-E}{R}\left(\frac{1}{T}-\frac{1}{T_o}\right)\right)$		
		k_f x 10^{10}	E_f (KJ/kmol)	n_f
23	$PZ - H_2O$	0.020	-17619	17.25
24	$PZ - PZCOO$	1.865	-35394	25.70
25	$PZ - PZ$	3.620	-116263	44.43
26	$PZ - CO_3^{2-}$	39.33	-54002	36.07
27	$PZ - OH$	46.75	-31303	23.83
28	$PZCOO - H_2O$	0.099	63251	-1.47
29	$PZCOO - PZCOO$	1.868	45476	6.98
30	$PZCOO - PZ$	3.628	-35394	25.70
31	$PZCOO - CO_3^{2-}$	19.36	26868	17.35
32	$CO_2 - OH\ (HCO_3^-)$	0.0009298	77495	-3.05
33	$PZ - CO_2\ (HCO_3^-)$	2.68 x 10^{-6}	-5086	17.55
34	$PZCOO - CO_2\ (HCO_3^-)$	1.98 x 10^{-6}	75784	-1.18

Table 5. Reverse 5mK$^+$/2.5mPZ Activity-Based Rate Parameters for Piperazine, Piperazine, and Bicarbonate Reaction as Inputted into AspenPlus® RateSep™

Eqn No.	Reaction	$Rate_{rev} = k\left(\frac{T}{T_o}\right)^n \exp\left(\frac{-E}{R}\left(\frac{1}{T}-\frac{1}{T_o}\right)\right)$		
		k_r	E_f (KJ/kmol)	n_f
35	$PZ - H_2O$	4.6302 x 10^{12}	185406	-33.04
36	$PZ - PZCOO$	2411	214987	-24.59
37	$PZ - PZ$	682	364854	-75.65
38	$PZ - CO_3^{2-}$	7623	252380	-49.70
39	$PZ - OH$	0.0352	283511	-48.94
40	$PZCOO - H_2O$	5.6615 x 10^{13}	79780	-1.47
41	$PZCOO - PZCOO$	59954	109361	6.98
42	$PZCOO - PZ$	16960	259228	-44.08
43	$PZCOO - CO_3^{2-}$	93182	146755	-18.14
44	$CO_2 - OH\ (HCO_3^-)$	0.00358	88750	11.25
45	$PZ - CO_2\ (HCO_3^-)$	0.06033	172473	-15.45
46	$PZCOO - CO_2\ (HCO_3^-)$	0.19661	22606	35.61

Absorber Model Validation

The absorption of CO_2 into the potassium carbonate/piperazine solvent occurs by mass transfer with fast chemical reaction. For rate-based reaction, if given enough time, the reaction should theoretically approach equilibrium. Therefore, for a given segment in an absorber column, the composition at the outlet should approach the equilibrium composition. The RateSep™ absorber model was validated by flashing the outlet stream of 0.3 meter high column and comparing the composition. The diameter of the column was set to 0.43 meters and contained Flexipac 2Y structured packing. It is expected that the ratio of concentration ratio of the species from the rich stream should match that of the flashed stream. At a liquid holdup of 2%, the absorber rich stream matches that of the flash stream, which is in equilibrium (Table 6). For a low liquid holdup, which is representative of a short reaction time, the concentration ratios do not match.

Table 6. Equilibrium Comparison between Absorber Rich Stream and Flashed Rich Stream

Rate Eqn (Activity)	Equil Flash	Abs Rich 2% Holdup	Abs Rich 0.0002% Holdup
$\frac{HCO_3 \cdot H_3O}{CO_2}$	1.06×10^{12}	1.06×10^{12}	7.31×10^{12}
$\frac{PZCOO \cdot H_3O}{CO_2 \cdot PZ}$	7.44×10^{-6}	7.44×10^{-6}	8.11×10^{-4}
$\frac{PZCOO_2 \cdot H_3O}{CO_2 \cdot PZCOO}$	1.05×10^{-6}	1.04×10^{-6}	1.13×10^{-4}

Conclusion and Future Work

It was found that continuing to treat the HPZCOO ion as a molecule within AspenPlus® was the best solution for reconciling the heat of absorption inconsistency. The heat of formation for the HPZCOO species was entered as DHFORM and the heat capacity parameters were entered into CPIG. In addition, HPZCOO was given a zero Watson Heat of Vaporization by entering 0 into the DHVLWT parameters. After the heat of absorption problem was solved, the concentration-based kinetics developed by Cullinane were converted to activity-based kinetics and inputted using the AspenPlus® power law format. Finally, the model was validated through a flash calculation of the rich outlet stream.

The absorber model is currently being validated with the pilot plant data from the final K^+/PZ campaign. The reconciliation process will utilize the data fit regression package found in AspenPlus®. The Aspen data fit regression package allows the user to input the raw data and assign a standard deviation to the individual data point. The input parameters will include the inlet gas and liquid rate, compositions, and temperatures. Also, the temperature profile across the column will be included. The adjustable parameters will include a gas factor and area factor. A working FORTRAN subroutine for the interfacial area has also been created. Based on some observations by the University of Texas at Austin – Separations Research Program, Frank Seibert has suggested using the specific area of the packing as the actual wetted area. The FORTRAN subroutine will allow the user to do this and additional adjustments to the kinetics/interfacial area will be done through an area factor in AspenPlus®.

Subtask 1.8a – Alternative stripper configurations – Aspen Custom Modeler for Stripper

by Babatunde Oyenekan

(supported by this contract)

A PhD dissertation and two paper manuscripts have been prepared on stripper modeling. The dissertation will be submitted as a DOE topical report in February 2007.

This work evaluates stripper performance for CO_2 capture using seven potential solvent formulations and seven stripper configurations. Equilibrium and rate models were developed in Aspen Custom Modeler (ACM). The temperature approach on the hot side of the cross exchanger was varied between 5 and 10^oC.

The results show that operating the cross exchanger at a 5^oC approach results in 12% energy savings for a 7m MEA rich solution of 0.563 mol/mol Alk and 90% CO_2 removal. For solvents with ΔH_{abs} < 60 kJ/gmol CO_2, stripping at 30 kPa is more attractive than stripping at 160 kPa. Normal pressure (160 kPa) favors solvents with high heats of desorption. The best solvent and process configuration, matrix with MDEA/PZ, offers 22% and 15% energy savings over the baseline and improved baseline, respectively, with stripping and compression to 10 MPa. The energy requirement for stripping and compression to 10 MPa is about 20% of the power output from a 500 MW power plant with 90% CO_2 removal.

Rate model results show that a 'short and fat' stripper requires 7 to 15% less equivalent work than a 'tall and skinny' one. The optimum stripper design could be one that operates between 50% and 80% flood at the bottom. Stripping at 30 kPa and 160 kPa require 230 s and 115 s of effective packing volume to get an equivalent work 4% greater than the minimum. Stripping at 30 kPa with $\Delta T = 5^oC$ was controlled by mass transfer with reaction in the boundary layer and diffusion (88% resistance at the rich end and 71% resistance at the lean end) and mass transfer with equilibrium reactions (84% resistance at the rich end and 74% resistance at the lean end) at 160 kPa.

The model was validated with data obtained from pilot plant experiments at the University of Texas with 5m K^+/2.5m PZ and 6.4m K^+/1.6m PZ under normal pressure and vacuum conditions using Flexipac AQ Style 20 structured packing. Foaming was experienced during tests. The effective packing height was 5.09m for 5m K^+/2.5m PZ and 6.47m for 6.4m K^+/1.6m PZ.

Subtask 1.9a – Economic Analysis – Stripper

by David Van Wagener

(supported by the Industrial Associates Program)

Introduction

This task will develop the heat and materials balances for a stripper using The PhD dissertation on this topic will be issued as a DOE topical report.

The stripper model already developed by Oyenekan incorporates several solvents including various concentrations of monoethanolamine (MEA) and potassium/piperazine (K^+/PZ) aqueous solutions. K^+/PZ has been determined to be an important solvent solution to study because it seems to outperform MEA in capacity and energy requirements in use for CO_2 removal by absorption/stripping.

K^+/PZ solutions have been modeled for 6.4m/1.6m, 5m/2.5m, and 4m/4m concentrations thus far (Oyenekan and Rochelle, 2006). The 4mK^+/4m PZ solvent has shown the most potential for energy efficiency, but it has been hypothesized that 4.5m/4.5m could have even better performance and CO_2 capacity. 4.5/4.5 is nearing the physical limit of the solubility of the salts, so higher concentrations will not be modeled.

Experimental

Two models written in Fortran code were used to obtain VLE and rate models for the solvent (Bishnoi, 2000; Cullinane, 2005). The thermodynamic VLE model calculated the equilibrium partial pressure of carbon dioxide (P_{CO2}*) for a given temperature (T) and loading of CO_2 in the liquid (γ). The rate model calculated k_g', the mass transfer coefficient in the liquid film layer. This value is a function of temperature, the loading of CO_2 in the liquid, the partial pressure of carbon dioxide at the surface of the liquid ($P_{CO2,i}$), and the mass transfer coefficient in the liquid (k_l).

Development of model for calculation of P_{CO2}*

The VLE model was run first. 470 data sets were constructed with a range of values for the dependent variables (T, loading)(Table 7). The VLE model calculated values for P_{CO2}* for each data set, and a regression was fit according to a previously derived correlation (Oyenekan, eq. 1). The values of the coefficients for the correlation are displayed below in Table 8, along with the corresponding standard errors and percent errors.

Table 7. VLE Model Variable Ranges

Variable	Low Value	High Value
Temperature	313K	413K
Loading	0.32	0.6

$$\ln P^*_{CO_2} = a + b\gamma + \frac{c}{T} + d\frac{\gamma^2}{T^2} + e\frac{\gamma}{T^2} + f\frac{\gamma}{T} \qquad (1)$$

Table 8. VLE Regression Coefficients

	Value	St. Error	% Error
a	7.21	1.44	19.9%
b	60.83	7.03	11.6%
c	-5116.22	656.84	12.8%
d	-4.71E+05	4.05E+05	86.0%
e	2.13E+06	8.17E+05	38.4%
f	-1.82E+04	4.73E+03	25.9%

The errors for several of the regression coefficients were very high, and analysis of the ratio of the calculated model values to the regression predicted values revealed unusual behavior of the value of P_{CO2}* for low loading (Figure 2). For this reason, a new regression was calculated while neglecting the data sets with low loading (γ <0.36). The coefficients for the regression of the modified data set are shown in Table 9.

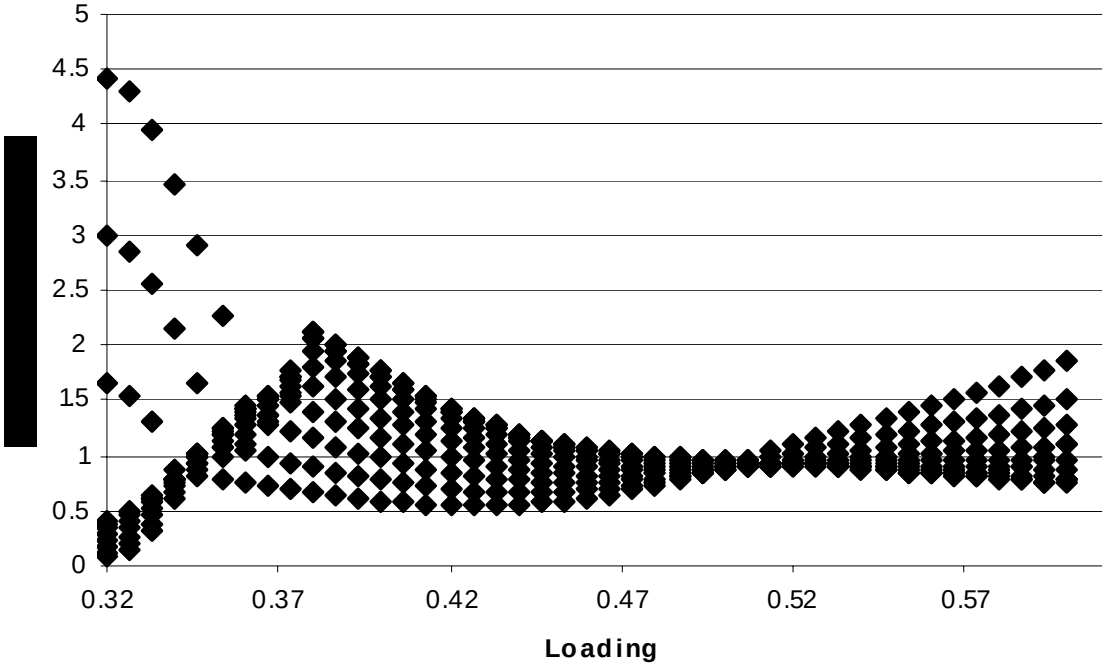

Figure 2. Calculated/predicted values for various loading values for VLE model, regression equation from Table 8.

Table 9. VLE Regression (Modified)

	Value	St. Error	% Error
a	17.25	0.61	3.51%
b	41.45	2.38	5.75%
c	-6572.07	295.21	4.49%
d	2.59E+06	1.81E+05	6.96%
e	5.69E+05	2.68E+05	47.02%
f	-1.56E+04	1.57E+03	10.07%

Development of model for prediction of k_g'

Following the successful run of the VLE model, a collection of 11,970 data points was constructed for the rate model. The same ranges of temperature and loading were used, and a range of values were also used for the remaining two dependent variables (k_l, $P_{CO2,i}$), see Table 10.

Table 10. k_g' Model Variable Ranges

Variable	Low Value	High Value
Temperature	313K	413K
Loading	0.32	0.6
k_l	1.00E-04	5.00E-04
$P_{CO2,i}$	0.1*P_{CO2}*	0.9*P_{CO2}*

Similar to the method for the VLE model, the values of k_g' calculated by the rate model were fit to a correlation developed by Oyenekan (eq. 2) (2006b). The values of the coefficients for the correlation are displayed below in Table 11, along with the corresponding standard errors and percent errors. The same decreased range of loading was used to avoid the unusual CO_2 partial pressure calculations. Additionally, data sets with very large values of P_{CO2} * (P_{CO2} *>1MPa) were eliminated in order for the model to run without encountering an overflow. The cut in data sets was justified because the low loading values and the high partial pressures are out of the desired operating range of the regression model in ACM.

$$\ln k_g' = \left[\begin{array}{l} A + (B\gamma) + \left(\frac{C}{T}\right) + \left(D\, k_l\right) + \left(E\ P_{CO2,i}\right) + \left(F\ \frac{\gamma}{T}\right) + \left(G\ \frac{k_l}{T}\right) \\ + \left(H\ \frac{P_{CO2,i}}{T}\right) + \left(I\ \frac{\gamma^2}{T}\right) + \left(J\ \frac{\gamma}{T^2}\right) + \left(K \frac{\gamma^2}{T^2}\right) \end{array} \right] \qquad (2)$$

Table 11. Rate Regression Coefficients

	Value	St. Error	% Error
a	-83.60	1.05	1.26%
b	40.48	4.64	11.46%
c	3.16E+04	3.83E+02	1.21%
d	6.01E-06	2.76E-07	4.60%
e	2.47E+04	3.54E+02	1.43%
f	4.35E+04	1.62E+03	3.73%
g	-9.87E+06	1.32E+05	1.34%
h	-2.61E-03	1.03E-04	3.95%
i	-0.239	0.005	2.07%
j	-2.29E+07	9.61E+04	0.42%
k	1.09E+07	1.85E+05	1.70%

The regression of the rate model calculations seems to be a good fit because the percent error for all coefficients is relatively small, and the distribution of the ratios of the calculated values to the regression predicted values is closely centered around 1, (Figure 3)

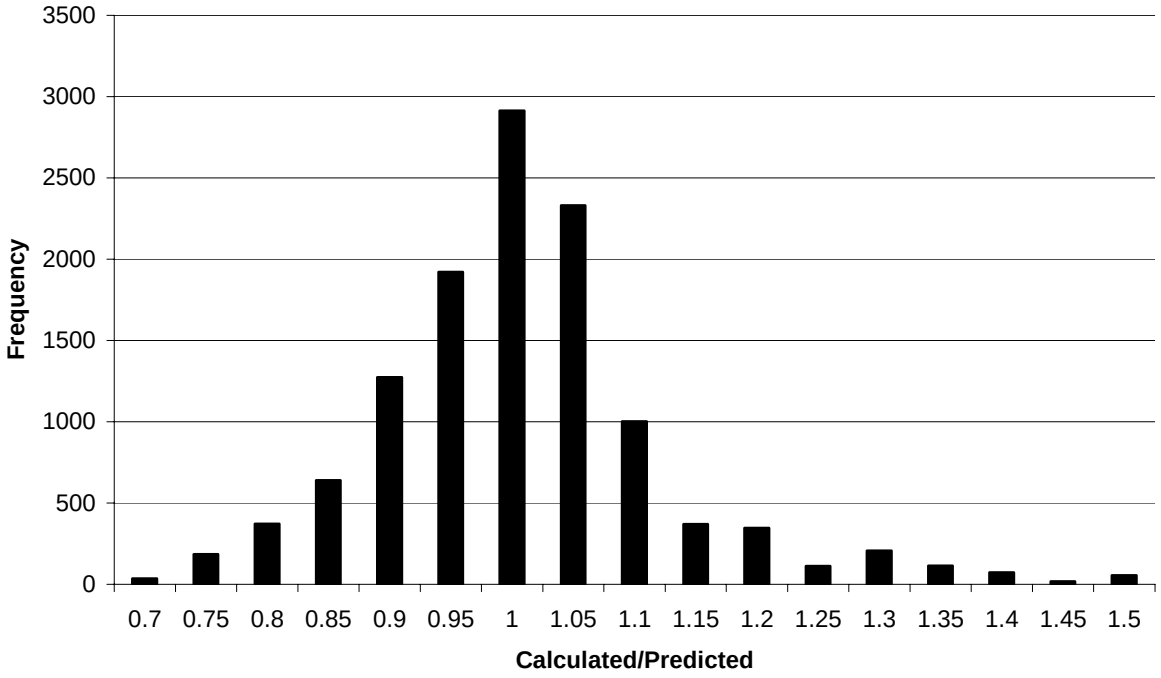

Figure 3. Distribution of calculated/predicted values for rate model

Conclusions and Future Work

The VLE model was run to create a closed form equation capable of predicting P_{CO2}* for a solution of 4.5mK^+/4.5mPZ. The model predicted values at the low end loadings did not fit the pattern of the rest of the calculations. Therefore, the final regression neglected the data sets with loadings smaller than 0.36 in order to yield a regression which can calculate the partial pressure within a small range of error. The rate model was also run to form a regression capable of predicting k_g' for the same solvent solution. The regression is accurate within the range of the dependent variables which was run.

The rate regression will be further developed to ensure that it can predict k_g' accurately for all values that ACM will need. The data sets used in the Fortran rate model will be expanded to cover a larger range of CO_2 partial pressures, as long as the program will still run. Additionally, the reason for the abrupt change in the value of P_{CO2}* calculated by the model at about $\gamma = 0.37$ will be investigated.

Subtask 1.9b – Economic Analysis – Absorber

by Jorge M. Plaza

(supported by the Industrial Associates Program)

Introduction

Cost estimates are being developed by Trimeric Corporation under a SBIR agreement with the DOE. In this task we are developing the modeling capability to provide heat and material balances for an absorber using 4.5 m K+/4.5 m PZ.

For the modeling task, Chen developed an absorber model for CO_2 absorption in Aspen RateSep™ using the VLE model generated by Hilliard. However, Chen observed that the developed model incorrectly predicted the heats of absorption so work was started to fix this issue. Furthermore, different compositions of the potassium carbonate/piperazine have been proposed for analysis. This report discusses work carried out on a 4.5/4.5 m potassium carbonate/piperazine, which is close to the limiting solubility for this system. Heats of absorption were calculated using AspenPlus® flash calculations for heat duty and compared to results obtained from the Clausius-Clapeyron equation using vapor data obtained from the Aspen flash simulations. The goal of this comparison was to verify that the incongruence found by Chen was solved and that the solution is applicable to the proposed concentration.

Additionally, results from AspenPlus® flash calculations were used to estimate activity coefficient based equilibrium constants for later use in modeling CO_2 absorption using the 4.5/4.5 potassium carbonate/piperazine solvent. Moreover, this initial task served as a training tool on the work carried out by Chen and on AspenPlus® and RateSep™ modeling.

Experimental

Heats of Absorption

Heats of absorption were estimated using flash calculations set up in AspenPlus®. As previously done by Chen, a gas stream containing pure CO_2 was put in contact with a liquid stream composed of potassium carbonate/piperazine (4.5/4.5 molal) and carbon dioxide. Conditions for this initial run are presented in Table 12. For this run a loading of 0.46 (CO_2/Total alkalinity) was used. Inlet flow of carbon dioxide was set at 1.56 moles/hr and the inlet solvent CO_2 flow was 2.4 moles/hr.

Table 12. Initial AspenPlus® flash calculation model run

T (^oC)	P_{CO2} (Pa)	Heat Duty (J/mol)	$\Delta H^{(1)}$ (J/mol)	Variation (%)
20.0	262.45	-89186.24	-81011.29	9.2
30.0	763.45	-86241.94	-78425.19	9.1
40.0	2010.36	-82866.70	-76120.78	8.1
50.0	4826.20	-79067.39	-73511.51	7.0
60.0	10620.94	-74841.89	-70568.45	5.7
70.0	21560.07	-70210.73	-67439.56	3.9

(1) This is the heat of absorption calculated using the Clausius-Clapeyron equation.

Aspen flash calculations were conducted at the temperatures in Table 12 and at 0.1^{o}C below them. This was done to estimate the heat of absorption using the Van Hoff equation as follows:

$$\frac{\ln P_{CO_2,T_2}}{\ln P_{CO_2,T_1}} = \frac{-\Delta H}{R}\left(\frac{1}{T_2} - \frac{1}{T_1}\right)$$

Results show a relative high deviation between AspenPlus® flash results and the Van Hoff equation. This deviation was related to the use of a high inlet flow in the pure carbon dioxide stream. The estimated values are not of a differential heat of absorption for carbon dioxide but

of an integral value. Changes in the flash model setup were conducted to take into account this observation. Table 13 shows the results for the AspenPlus® run using smaller carbon dioxide flow to obtain a differential heat of absorption. For this purpose CO_2 inlet flow was set at 0.101 moles/hr, CO_2 in the inlet solvent at 3.86 moles/hr, and loading remained at 0.46.

Table 13. Corrected AspenPlus® flash calculation model run

T (^oC)	P_{CO2} (Pa)	Heat Duty (J/mol)	$\Delta H^{(1)}$ (J/mol)	Variation (%)
20.0	263.18	-79658.27	-80980.63	1.7
30.0	765.31	-77048.27	-78400.17	1.8
40.0	2014.72	-74437.52	-74437.52	2.2
50.0	4835.68	-71593.62	-71593.62	2.7
60.0	10640.17	-68377.27	-68377.27	3.2
70.0	21596.68	-64795.97	-64795.97	4.1

(1) This is the heat of absorption calculated using the Van Hoff equation.

The results obtained with the corrected setup have a much smaller variation than the previous results, thus the corrections done by Chen seem to work for the proposed system.

Activity Coefficients and Equilibrium Constants

The AspenPlus® flash model calculation set up by Chen also estimates the activity coefficients for the species present in the system. A temperature of 40^{o}C was selected to calculate the equilibrium constants based on activity coefficients. This temperature is an average of the temperatures of the absorption system.

Table 14. Estimated activity coefficients (γ) at 40^{o}C

Compound	PZ	CO_2	HCO3	OH	H_2O	PZCOO
γ	0.6827	2.8685	0.1020	0.9727	0.9846	0.6834

Using the values obtained for the activity coefficients and an Excel tool developed by Chen, equilibrium constants were calculated for the following reactions. (Table 15 presents the results obtained for the equilibrium constants).

$$PZH^+ + H_2O \longleftrightarrow PZ + H_3O^+$$

$$PZ + HCO_3^- \longleftrightarrow PZCOO^- + H_2O$$

$$PZCOO^- + HCO_3^- \longleftrightarrow PZ(COO^-)_2 + H_2O$$

$$H^+PZCOO^- + PZ \longleftrightarrow PZCOO^- + PZH^+$$

Table 15. Calculated activity-based equilibrium constants at 40°C

Equilibrium Constant	$\ln K_{eq} = A + B/T + C\ln T$		
	A	B	C
$K_{PZH^+} = \frac{a_{PZ} \cdot a_{H_3O^+}}{a_{PZH^+} \cdot a_{H_2O}}$	-27.83	-33448.7	-69.78
$K_{PZH^+} = \frac{a_{PZCOO^-} \cdot a_{H_2O}}{a_{PZ} \cdot a_{HCO_3^-}}$	8.61	36511.7	87.06
$K_{PZH^+} = \frac{a_{PZ(COO^-)_2} \cdot a_{H_2O}}{a_{PZCOO^-} \cdot a_{HCO_3^-}}$	5.39	14080.2	36.78
$K_{PZH^+} = \frac{a_{PZCOO^-} \cdot a_{PZH^+}}{a_{PZCOO^-} \cdot a_{PZ}}$	1.92	27752.8	69.78

Conclusions

Results showed that corrections on the calculation of the heat of absorption by Chen are adequate and applicable to the proposed solvent concentration. However, there is still a small discrepancy between the data generated using AspenPlus® heat load and the Van Hoff equation.

Using the set up Aspen model and Chen's Excel tool it is possible to obtain the equilibrium constants and reaction rates for the solvent system under study. This will in turn allow modeling the absorption system with the proposed solvent.

Future Work

- Absorption modeling of the 4.5/4.5 system using the estimated constants. Initial modeling will be done for a fixed packing height of 15 m. Design specifications will be set up to obtain a 90% removal of CO_2. Lean loading will be varied to develop plots relating it to solvent rate and rich loading at a specific packing height. Additional modeling runs will be set up with different types of packing and plates to obtain loading plots relating solvent rate and rich loading.
- A new solvent system has been proposed using 5 molal piperazine. Equilibrium constants and all other required parameters will be calculated to run models using this solvent. Plots relating loading conditions and different packing will also be generated.
- A full set of calculations for the heats of absorption and equilibrium constants will be done by hand as a training tool. It will help troubleshoot the slight difference between AspenPlus® and the Clausius-Clapeyron equation as well as verify the Excel tool results.

Task 3 – Solvent Losses

Subtask 3.1 – Analysis of Degradation Products

by Andrew Sexton

(supported by the Industrial Associates Program)

Introduction

This effort is an extension of work by George Goff on the oxidative degradation of MEA. Goff showed that oxidative degradation, under high catalyst conditions, is mass-transfer limited by the physical absorption of O_2 into the amine and not by reaction kinetics. Goff also theorized that the oxidative degradation of MEA produced volatile ammonia as well as a host of other proposed degradation products. The major degradation products among these include the heat stable salts of carboxylic acids, nitrite, and nitrate.

The oxygen stoichiometry necessary to produce these degradation products varies for each individual component; overall, it varies anywhere from 0.5 to 2.5 (Goff, 2004). It is believed that the particular degradation products are specific to certain metal catalysts present in the absorption/stripping system – specifically iron and copper. For example, the following balanced reactions illustrate the differences in oxygen consumption based on the end products:

$$MEA + 1.5\ O_2 \rightarrow 2\ Formate + Ammonia$$

$$MEA + 3.5\ O_2 \rightarrow 2\ Formate + Nitrate + Water$$

$$MEA + O_2 \rightarrow Glycolate + Ammonia$$

Goff's work on MEA degradation was limited to analyzing MEA degradation rates via the evolution of NH_3. The ammonia evolution rates were measured using a Fourier Transform Infrared (FT-IR) analyzer.

This effort extends Goff's gas-phase analysis by applying various methods of liquid-phase analysis, specifically ion chromatography and nuclear magnetic resonance. These analytical methods will be used to quantify the rate of amine degradation as well as the rate of degradation product formation for amine systems.

Since most gas treating processes using alkanolamines for CO_2 removal are performed in the absence of oxygen, oxidative degradation is a source of solvent degradation that has not been properly quantified. Oxidative degradation is important because it can impact the environment, process economics and decrease equipment life due to corrosion.

The environmental effects refer to the degradation products themselves: what is being produced, how much of it is being produced, and how can it be disposed of without doing significant damage to the environment. Process economics being impacted are the solvent make-up rate and design of the reclaiming operation. If amine is continually being degraded, then fresh amine must be continually added to the process at a significant cost. In addition, CO_2 loaded amine solutions corrode carbon steel equipment, which catalyzes oxidative degradation even further. It is imperative to quantify how much of this solvent make-up rate is due to oxidative degradation.

Experimental

As stated in prior reports, ion chromatography is the most extensively used liquid-phase analytical method. Anion chromatography utilizes an AS15 (a low-capacity column designed to separate low-molecular weight anions, specifically acetate, glycolate, and formate) IonPac column and an ASRS 4-mm self-regenerating suppressor made by Dionex, while cation analysis uses a CS17 and a CSRS 4-mm self-regenerating suppressor. Anion analysis employs a linear gradient of NaOH eluent, while cation analysis uses a constant concentration methanesulfonic acid (MSA) eluent. Refer to the June 2006 quarterly report for a detailed explanation of the analytical methods.

While experiments in this quarter were performed only on the low gas flow experimental apparatus, both the low and high gas flow experimental apparatuses have been modified. As noted in previous reports, the high gas flow setup uses a reaction gas mixture of air, CO_2, and N_2 (to dilute oxygen concentration to 15% O_2 on a wet basis) bubbled through water, which pre-saturates the gas before it is sparged thorough the amine solution in the reactor. The pre-saturator is a stainless steel calorimetric bomb located in separate heat bath, which consists of water kept at 55^{o}C (Goff, 2005).

A constant temperature of 55^{o}C is maintained in the reactor by circulating a silicone-based heat transfer fluid through the jacketed portion of the 1-L glass reactor. The entire reactor is well insulated in order to minimize heat loss to the environment. A stainless steel shaft and impeller, controlled at approximately 1400 RPM, keeps the amine solution in the reactor well-mixed. A heated sample line connected to the top of the reactor directs the vapor from the apparatus into the Temet Gasmet^{TM} Dx-4000 FT-IR analyzer. The FT-IR can analyze up to 50 components; the most important one in this case is ammonia evolution from the reactor apparatus. This allows us to assume an amine degradation rate. Refer to Chapter 3 of Goff (2005) for a more in-depth explanation of how this apparatus operates.

The modifications to the apparatus, as detailed in Figures 4 through 6, were made on the stainless steel calorimeter bomb, which serves as the presaturator. Figure 4 illustrates the presaturator prior to the modifications (all high gas flow experiments up to this point have been run under this configuration). The sealed bomb has two openings on top – one for the dry gas inlet from the mass flow controllers and the other for the saturated gas outlet to the reactor. 150ml of distilled, deionized water is poured into the bomb prior to the beginning of the experiment.

Once the bomb is sealed, and the experiment begins, dry gas is bubbled through a dip tube that carries the gas to the bottom of the reservoir. The gas bubbles up through the heated water and saturated vapor (at 55^{o}C) exits the presaturator to the reactor. As gas is continually passed through the bomb, the evaporation of water lowers the level in the bomb. Therefore, in order to avoid running the presaturator dry and sending dry gas to the reactor (which decreases the temperature in the reactor and disrupts the water balance), water is continuously added to the presaturator. Water is added through a rubber septum once a valve upstream of the bomb is opened.

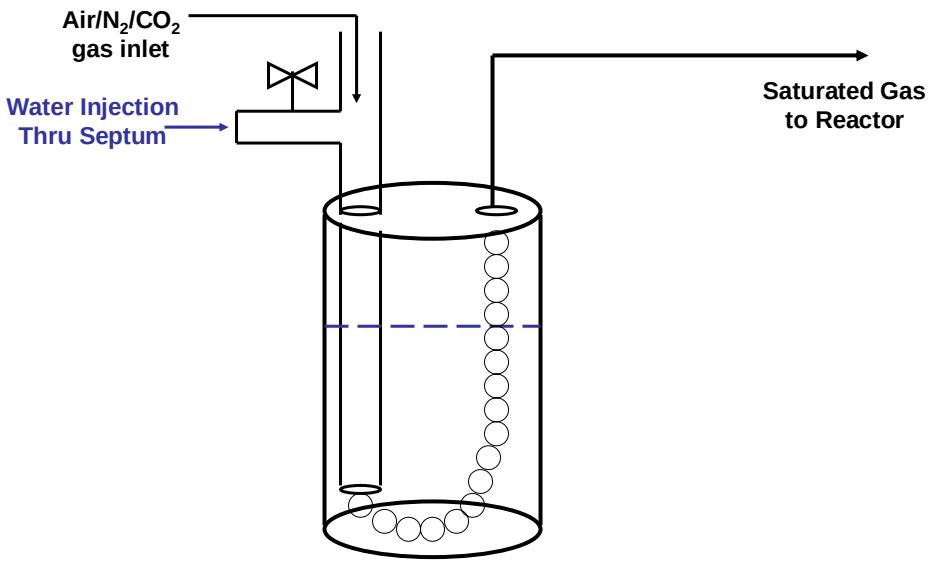

Figure 4. Original Configuration for High Gas Flow Presaturator

The manual addition of water to the high gas flow apparatus proves to be a problem. The high gas flow apparatus was developed for gas-phase analysis of degradation products. The length of an experiment is limited by manpower: as long as someone is present to manually inject water into the presaturator every hour, then the water balance can be maintained and the results of the experiment are viable.

Typically, the high gas flow experiments are performed by one person and last a maximum of 18 hours. However, 18 hours is not long enough to accumulate a significant amount of liquid-phase degradation products. An experiment on the order of a week would be a more acceptable time period to degrade the amine. An automatic control system on the water level in the presaturator would achieve this.

Two additional connections were machined in the top of the presaturator for a water inlet and outlet. Water flow in and out of the presaturator is controlled by Masterflex rotary peristaltic pumps. A peristaltic pump is a positive displacement pump in which the fluid is contained within a flexible tube fitted inside a circular pump casing. Peristaltic pumps are advantageous because they are inexpensive, easy to maintain, and they will not cavitate because the fluid never comes into contact with the inner workings of the pump.

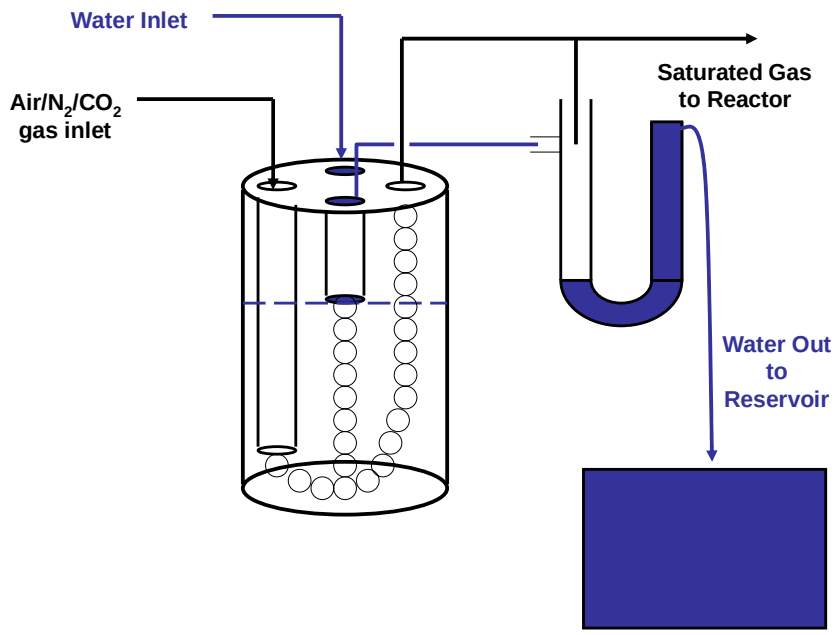

Figure 5. Modified Configuration for High Gas Flow Presaturator

A Masterflex pump head sized for 1/16" flexible tubing was used on the inlet, while a pump head sized for 1/8" tubing was used on the outlet. Using larger tubing on the outlet guarantees that the inlet water flowrate will be less than the flow out. A stainless steel dip tube was cut so that its length is one-third of the depth of the presaturator. Both pump heads run continuously.

The inlet pump delivers distilled, deionized water into the presaturator at a rate of approximately 1ml/min. This is greater than the evaporation rate of water to the reactor, which is 0.5ml/min. The outlet pump is set at 4ml/min. When the water level is below the dip tube, the pump pulls from the vapor space in the presaturator. Once the water reaches the level of the dip tube, as shown in Figure 5, the pump will remove water along with the vapor. With this setup, the presaturator should never run dry or flood.

In order to keep any gas from escaping the closed system, the water outlet tubing will connect to a ½" Tygon tube configured into a U-shape. Once the tube expands from 1/8" to ½", the liquid will fall to the bottom of the tube while the gas rises up the tube. The gas will reconnect to the gas line out of the presaturator to the reactor, while the excess water will go to a large collection reservoir.

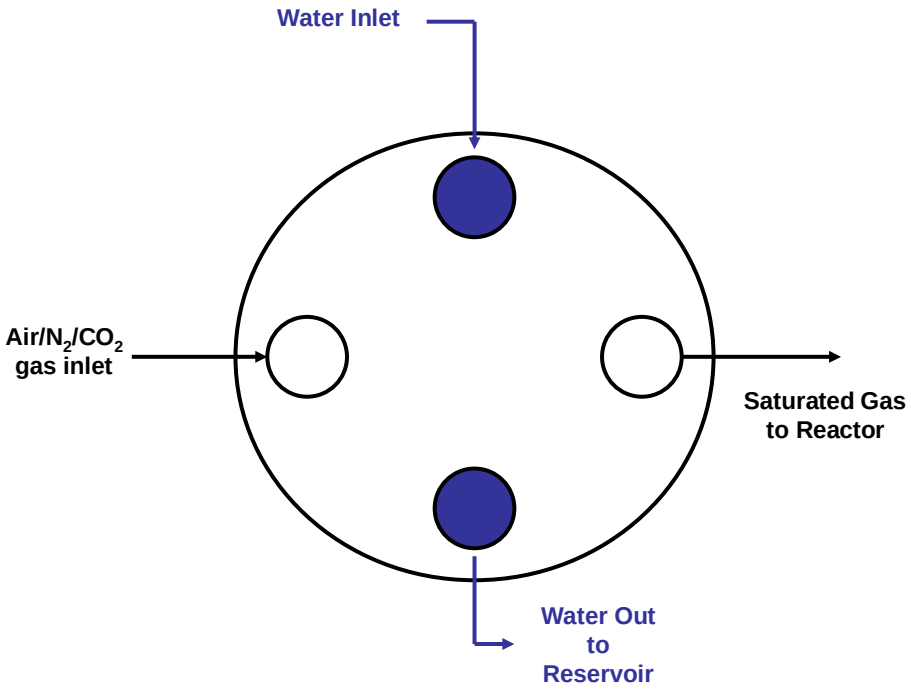

Figure 6. Top View of Modified High Gas Flow Presaturator

As described in previous reports, amine solutions in the low gas flow degradation apparatus are oxidized for 12 to 14 days in a low-gas flow jacketed reactor at 55°C. The solutions are agitated at 1400 RPM to produce a high level of gas/liquid mass transfer by vortexing. 98% O_2/2% CO_2 at 100ml/min is introduced across the vortexed surface of 350ml of aqueous amine. Samples were taken from the reactor at regular intervals in order to determine how degradation products formed over the course of the experiment. Prior quarterly reports provide a detailed explanation of the low gas flow degradation apparatus.

The modification to the low gas flow apparatus is illustrated in Figures 7 and 8. The difference in the figures is highlighted by the dashed box. The original configuration, as shown in Figure 7, used an inlet gas of 98% O_2/2% CO_2 premixed in a cylinder provided by Praxair. A Cole-Parmer rotameter was used to control the flowrate at approximately 100ml/min.

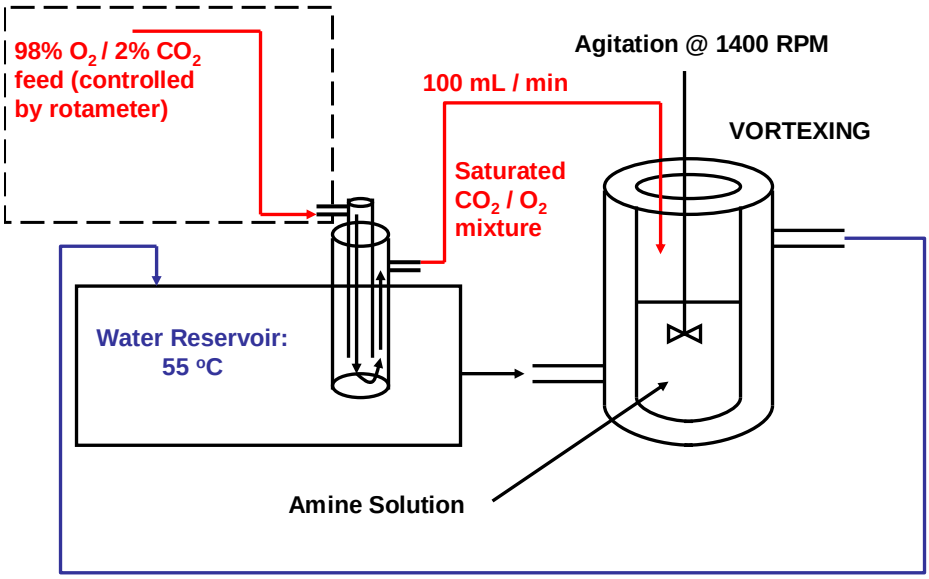

Figure 7. Original Configuration for Low Gas Flow Apparatus

The modified configuration still utilizes cylinders provided by Praxair – a pure oxygen cylinder and a pure CO_2 cylinder. The 98% O_2/2% CO_2 mixture is achieved using a 4 channel Brose box made by Brooks and two mass flow controllers made by Aera. Oxygen flowrate is controlled by a 200cc flow controller, while carbon dioxide is controlled by a 10cc flow controller. The control box displays a digital readout corresponding to the % open of the mass flow controller.

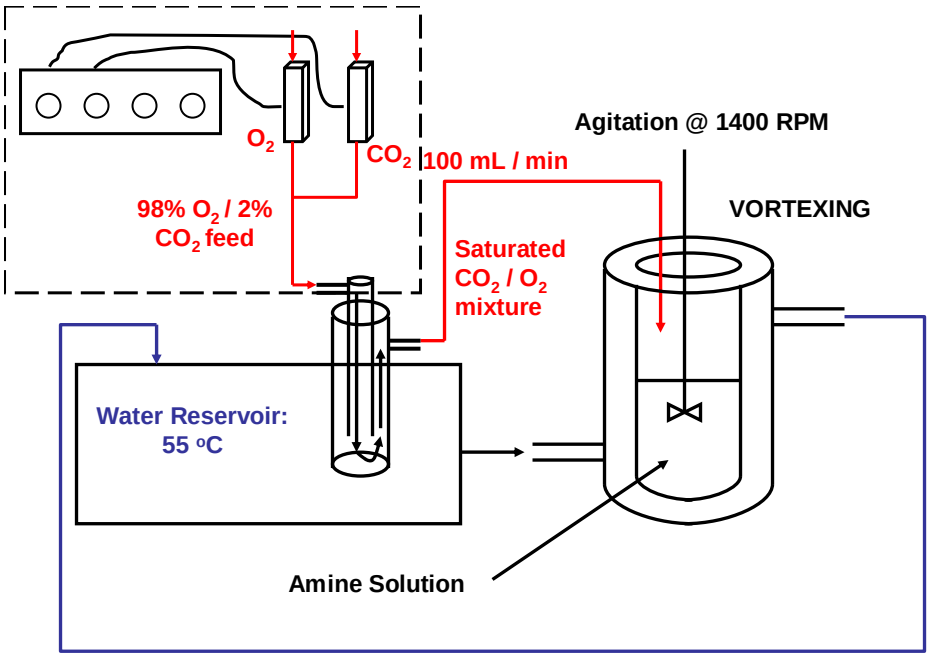

Figure 8. Modified Configuration for Low Gas Flow Apparatus

One issue arose while constructing the flow control system for the low gas flow apparatus. The Aera mass flow controllers were wired with male 20-pin Honda connectors (Figure 9), while the control box was equipped with female 15-pin D connections (Figure 10). First, the function of each pin for both of the connectors was determined from company literature. Then, with the assistance of Mark Phillips of the mechanical engineering department, the wires were stripped on the flow controllers and the Honda connectors. Subsequently, 15-pin male D connectors were soldered on in place of the Honda connectors with the pin function that matched the female connections on the control box.

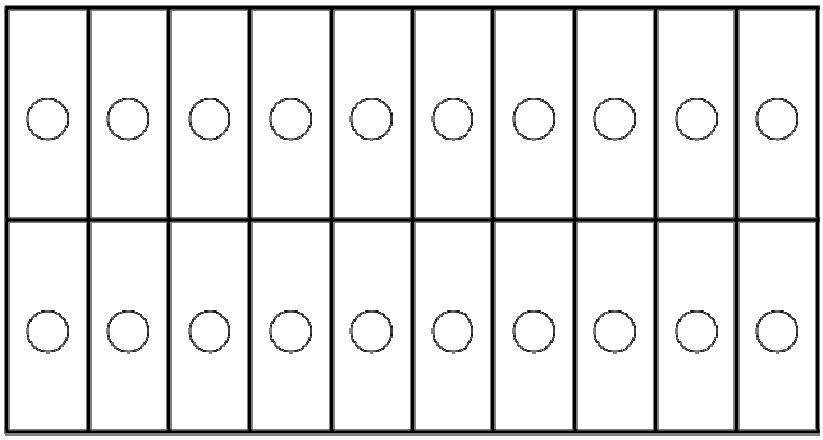

Figure 9. 20-Pin Honda Connector for Aera Mass Flow Controllers

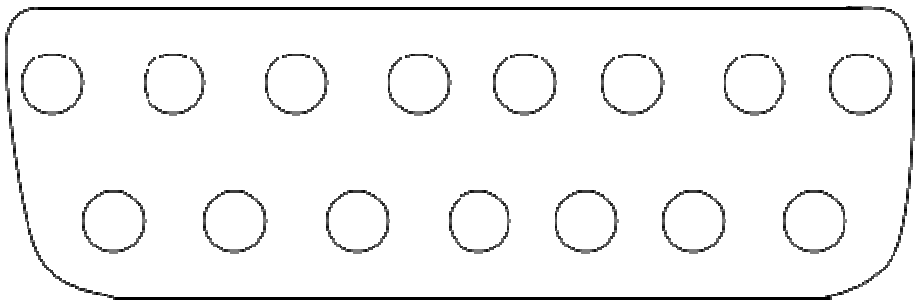

Figure 10. 15-Pin D Connectors for Control Box

Results

Using the analytical methods for the AS15 and CS17 columns, the following degradation experiments are being analyzed for degradation product formation rates:

1. November 2006 PZ experiment (Oxidative degradation of 2.5 m PZ/5 m $KHCO_3$, 55^oC, 1400 RPM, 500 ppm V, 98%O_2/2%CO_2).

2. December 2006 PZ experiment (Oxidative degradation of 2.5 m PZ, 55^oC, 1400 RPM, 100 mM "A", 500 ppm V, 98%O_2/2%CO_2).

Analysis was completed on these experiments, which were conducted during the prior quarters:

3. September 2006 MEA experiment (Oxidative degradation of 35 wt % MEA, 55^oC, 1400 RPM, 5 ppm Fe, 0.4 moles CO_2/mol MEA, 98%O_2/2%CO_2).

4. September 2006 MEA/PZ experiment (Oxidative degradation of 7 m MEA / 2 m PZ, 55^oC, 1400 RPM, 5 ppm Fe, 250 ppm Cu, 98%O_2/2%CO_2).

Table 16 lists oxidative degradation product formate rates for the two September low gas flow degradation experiments, while Table 17 compares them to similar experiments run in the past. The 35 wt % MEA experiment (Figure 11) represents an uninhibited commercial system in which iron is continually removed from the absorber/stripper system. The MEA/PZ experiment (Figure 12) represents a commercial system in which Cu is added as a corrosion inhibitor. As in prior experiments, formate is the most abundant degradation product for both experiments.

Table 16. Low Gas Flow Degradation Product Rates

Distinguishing Conditions	35 wt % MEA, 5 ppm Fe	7 m MEA/2 m PZ, 5 ppm Fe, 250 ppm Cu
Formate	0.36	0.83
Acetate	0.17	0.68
Oxalate	0.04	0.13
Nitrate	0.04	0.07
Nitrite	0.14	-

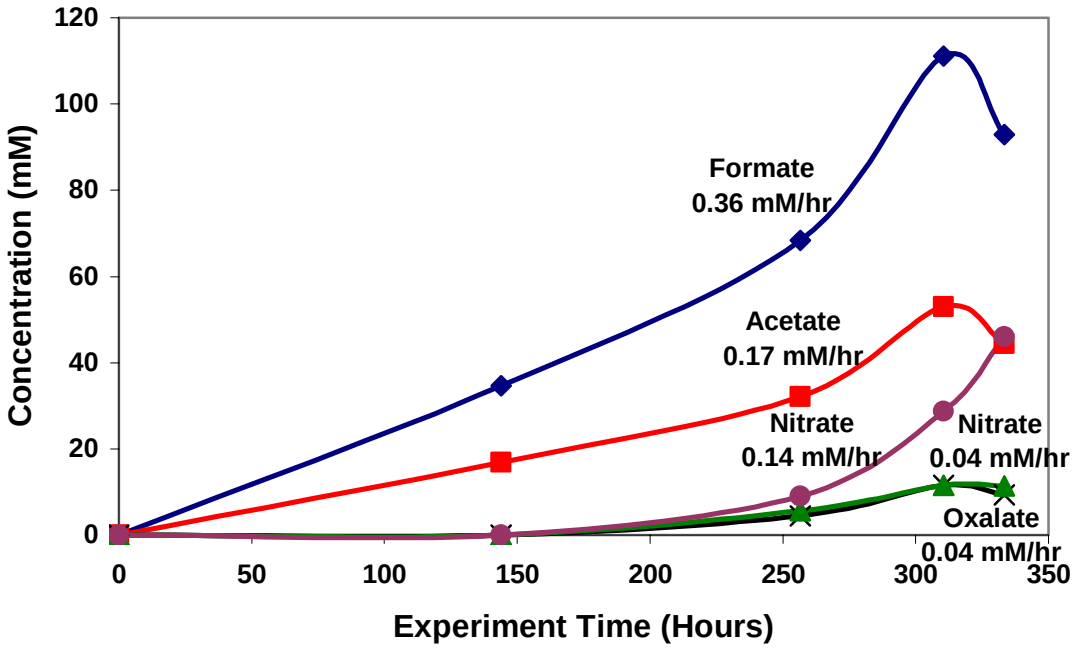

Figure 11. September 2006 MEA experiment (35 wt % MEA, 55°C, 1400 RPM, 5 ppm Fe, 0.4 moles CO_2/mol MEA, 98%O_2/2%CO_2)

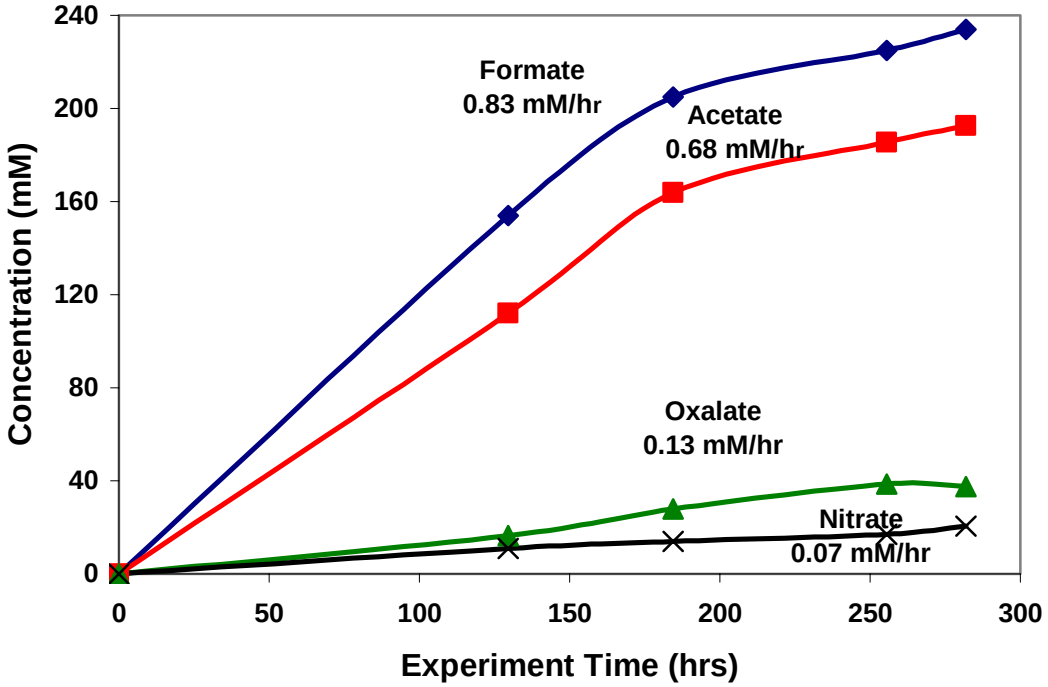

Figure 12. September 2006 MEA/PZ experiment (7 m MEA/2 m PZ, 55°C, 1400 RPM, 5 ppm Fe, 250 ppm Cu, 98%O_2/2%CO_2)

Table 17. Comparing Degradation Rates with Prior Experiments

Distinguishing Conditions	35 wt % MEA, 5 ppm Fe	30 wt % MEA, 250 ppn Fe	7 m MEA/2 m PZ, 5 ppm Fe, 250 ppm Cu	7 m MEA/2 m PZ, 5 ppm Fe
Formate	0.36	0.40	0.83	0.04
Acetate	0.17	0.02	0.68	-
Oxalate	0.04	0.04	0.13	-
Nitrate	0.04	0.15	0.07	0.02
Nitrite	0.14	0.31	-	0.003

It is difficult to draw any results from these comparisons. No other 35 wt % MEA experiments have been performed in the low gas flow apparatus; moreover, no 30 wt % MEA experiments have been performed at iron concentrations below 250 ppm. However, it seems that the effect of increasing the MEA concentration offsets the effect of lowering the iron concentration. Degradation rates are slightly lower for the 35 wt % MEA experiment, but they are on the same order of magnitude.

For the MEA/PZ experiments, adding 250 ppm Cu catalyzed the amine degradation significantly. Formate degradation increased by a factor of 20 when Cu was added to Fe. This is consistent with findings of MEA only experiments. During this quarter, the cation suppressor was malfunctioning; none of the cation data is reliable and the suppressor has been replaced. At this time, it is not clear if any EDA was formed from the most recent MEA/PZ experiment.

Therefore, we do not know if any piperazine was degrading during this experiment. Complete analysis will be included in the next quarterly report.

Although no numbers are reported here, early analysis of the November 2006 low gas flow degradation experiment appears to show the same results as the May 2006 experiment. All anionic degradation products appear to have a formation rate of less than 0.01 mM/hr. Since the anionic samples were not duplicated and cation analysis has not been performed yet, I refrained from publishing the numbers until next quarter.

Conclusions and Future Work

It is difficult to draw many conclusions from the experiments this quarter, because some of the analysis is still incomplete. Conclusions that can be drawn from analysis of these experiments will be included in the next quarterly DOE report.

With respect to the next two quarters, there are two major blocks of unfinished work that need to be completed. A lot of data has been collected over the past year and a half, but it lacks cohesion. Separating the project into blocks will make it easier to answer these questions.

The first block involves oxidative degradation under mass-transfer controlled conditions. More specifically, what are the effects of Fe only, Cu only, and Fe/Cu combined on MEA systems, PZ systems, and PZ/K systems? Furthermore, what are the effects of V on MEA systems and PZ/K systems?

The other major block of work involves competitive degradation. In other words, when solutions of MEA/PZ are degraded, which one degrades faster? Is piperazine degradation protected by the MEA? How do rates compare to MEA only solutions at similar conditions?

Blocks of experiments in the modified high gas flow experimental apparatus have been created to answer these questions. Modifying the high gas flow apparatus to identify liquid-phase and gas-phase products will allow us to account for all major degradation products and close the material balance so that we can account for everything. Some of these experiments will be run in parallel in the low gas flow degradation apparatus.

In addition, I am in the process of purchasing a column(s) that will detect species that pass through the current columns undetected. These species included aldehydes (formaldehyde and acetaldehyde) and amino acids (bicine and glycine).

Subtask 3.3 – Thermal Degradation

by Jason Davis

(supported by the Industrial Associates Program)

Introduction

This subtask will be used to define future work for the development of a kinetic model for MEA thermal degradation by carbamate polymerization. While the initial products of thermal degradation have been identified, the kinetics of the thermal degradation pathways have not been clearly defined. Currently, MEA concentrations are capped at 30 wt % to minimize thermal degradation and prevent corrosion in industrial applications; however, with a better understanding of degradation kinetics, this number can be optimized. This work will also allow us to better understand solvent losses by thermal degradation.

Theory

Polderman, Dillon and Steele (Polderman, Dillon, et al., 1955) describe the mechanism for thermal degradation by carbamate polymerization. In CO_2 capture, MEA associates with CO_2 in the absorber to form MEA carbamate as illustrated below.

This reaction is normally reversed in the stripper, but in some cases the MEA carbamate will polymerize to form 2-oxazolidone, which is also a reversible reaction, as shown below.

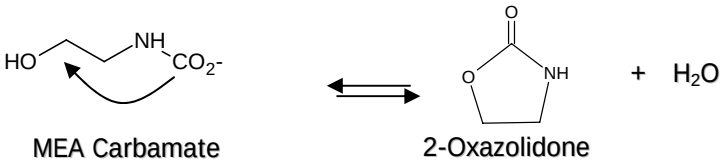

MEA carbamate can also irreversibly dehydrolize to form N,N'-di(2-hydroxyethyl)urea(Yazvikova, Zelenskaya, et al., 1975).

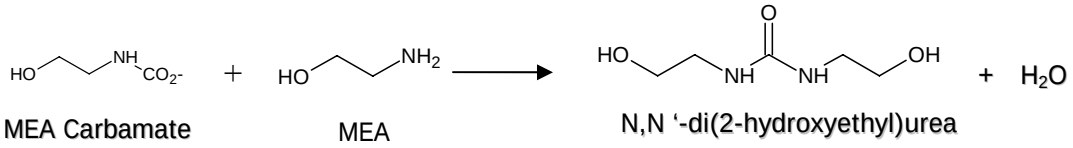

The former product, 2-Oxazolidone, can then react with another molecule of MEA to form 1-(2-hydroxyethyl)-2-imidazolidone which is sometimes referred to as HEIA.

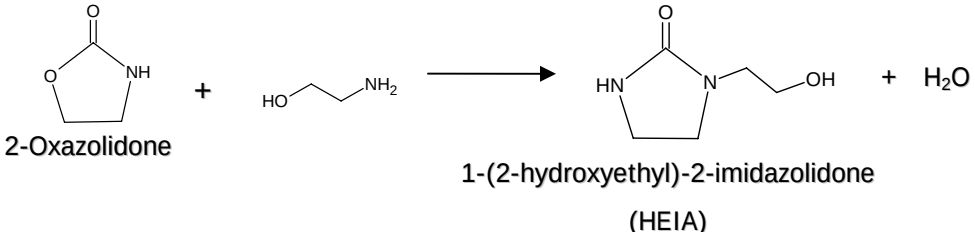

HEIA can then be hydrolyzed to form N-(2-hydroxyethyl)-ethylenediamine or HEEDA.

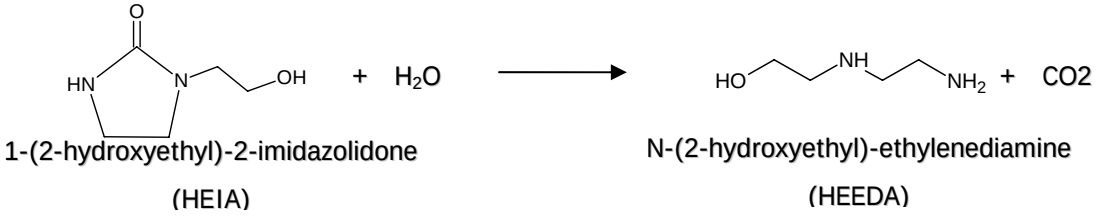

These four species (2-oxazolidone, dihydroxyethylurea, HEIA and HEEDA) are believed to be the main products of thermal degradation. The rate of formation of these products is a function of temperature (faster kinetics), CO_2 loading (more carbamate present), and MEA concentration.

Methods

High Temperature Experiments with Polar Column

A set of 5-2ml sample bombs were constructed using 316L SS tubing and Swagelok fittings. These bombs were filled with an amine solution and placed in a Stabil-Therm constant temperature cabinet made by Blue M for temperature control. The temperature was monitored periodically.

An HP5890 gas chromatograph was acquired and reconditioned complete with a 7673A automatic sampler and equipped with FID and TCD detectors. Based on a paper by Dawodu and Meisen (1993) and another paper by Supap, et al. (2006), a polar column was selected for the method development which follows the standard practice of polarity matching of the column to the analyte of interest. The column selected was the HP-Innowax column (30m x 0.25mm ID x 25um film thickness). The inlet and FID detector were maintained at 250^{o}C and the oven temperature was increased from 80^{o}C to 240^{o}C at a rate of 7^{o}C/min and held at the maximum temperature for 10 minutes. The carrier gas was helium and was used to maintain the pressure in the column at 25psig with a split ratio of 30:1. The split flow was determined by using a bubbler attached to the purge flow and measuring the column flow by injecting a nonretained organic solvent (hexane) and dividing the known column volume by the retention time.

A second column and method were used later in the experiments. The Agilent HP-5 column (30m x 0.53mm x 1.50um film thickness) was selected and the temperature profile was modified to start at 80^{o}C and increase to 250^{o}C at a rate of 10^{o}C/min. The column pressure was maintained at 20psig and all other parameters were held constant as compared to the previous method.

7m MEA solutions were made using Huntsman MEA and deionized water and were loaded to 0.4 mol CO_2/mol amine. 2ml of this solution was placed in each of the five sample bombs and placed in the Stabil-Therm oven and held at 150^{o}C. Samples were removed over the course of several weeks, diluted, and injected onto the GC for analysis.

Low Temperature Experiments

A set of sample bombs were constructed similar to the high temperature experiments. This time a matrix of MEA concentrations and loadings were used. Solutions of 3.5m, 7m, and 11m MEA were loaded to 0.2, 0.4, and 0.5 moles CO_2 per mole amine and loaded into a Stabil-Therm oven held at 100^{o}C. Samples were pulled at 1 and 2 weeks with longer hold times of 4, 6, and 8 weeks to be included in future reports. Samples were diluted 5:1 by weight with DI water before being injected on the HP-5 GC column.

Results and Discussion

High Temperature Experiments

A set of 7 m MEA samples spiked with known degradation products were prepared and injected onto the column. The following figure shows a sample spiked with 10 wt % oxazolidone and 10 wt % HEEDA.

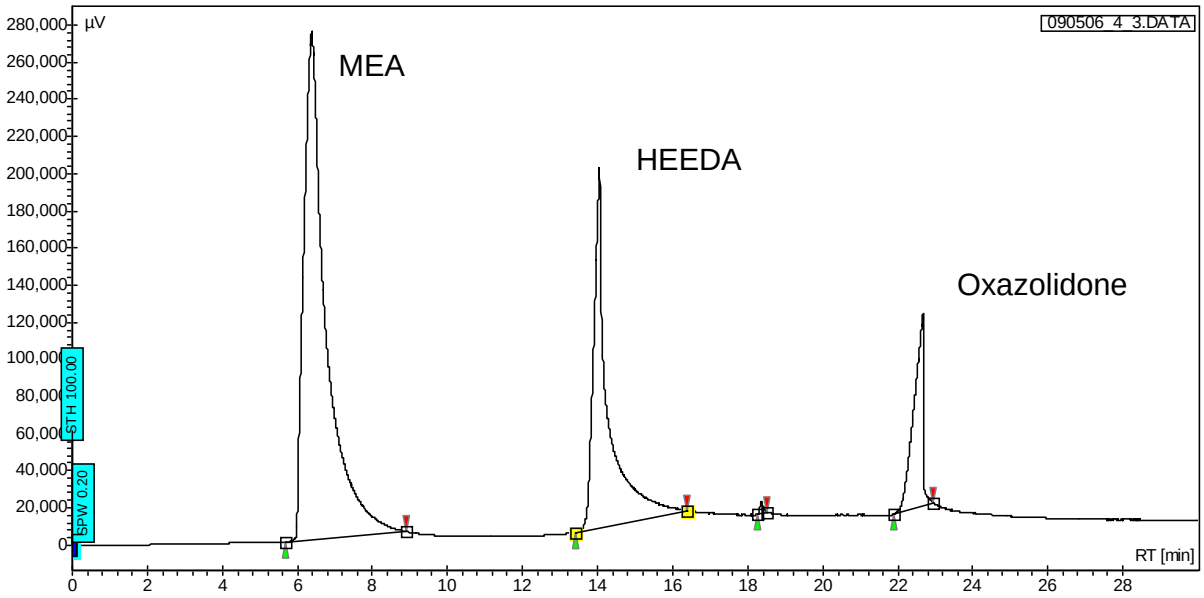

Figure 13. 7M MEA spiked with known thermal degradation products

The small peak at 18.5 minutes is associated with the oxazolidone peak. The relative area percents of the MEA, HEEA, and oxazolidone were 62, 28, and 10 percent respectively. From this we can say that the response factor for HEEDA is greater than MEA and oxazolidone and the response factor for oxazolidone is greater than MEA. The small peak at 18.5 minutes (0.2A%) is associated with the oxazolidone standard.

A solution of 7 m MEA loaded with 0.4 moles CO_2 per mole MEA was loaded into the sample bombs. They were placed in the oven set at 150°C and one sample bomb was removed every week. The samples were diluted with DI water to the desired concentration and 1uL was injected on the GC for analysis. The graph below shows the week 3 sample injection.

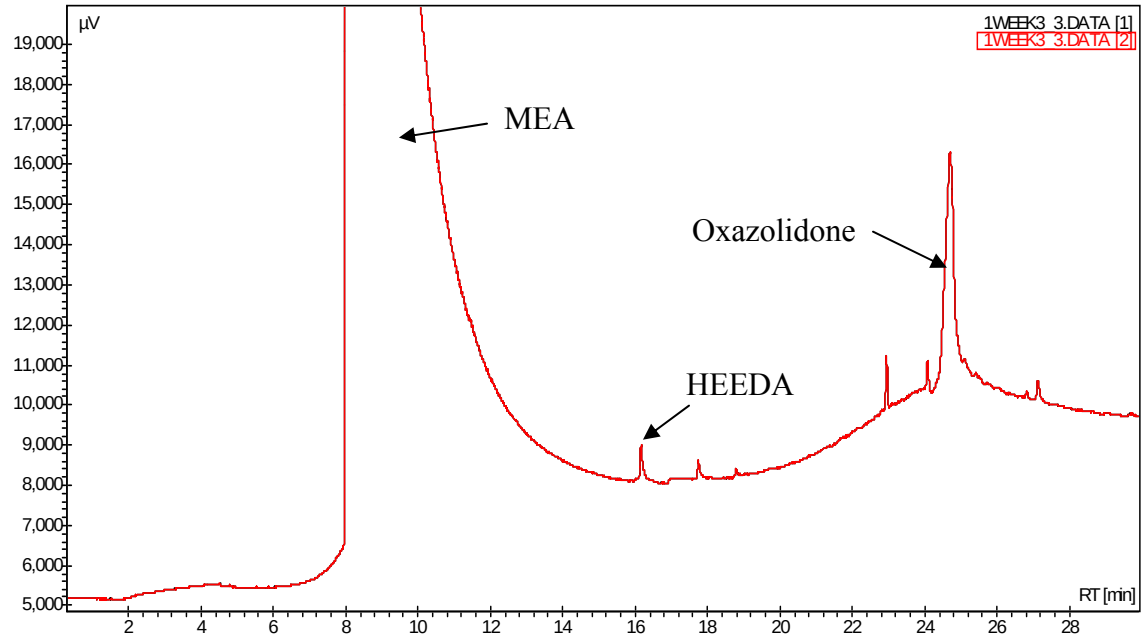

Figure 14. GC chromatogram of MEA solution held at 150°C for 3 weeks

The oxazolidone in this chromatogram makes up 0.75A% and the HEEDA peak amounts to 0.03A%. A 2-minute initial loading time has been added to the method where the temperature is maintained at 100°C as compared to Figure 13, which accounts for the 2-minute shift of all the peaks. There is a large baseline shift and significant tailing from the MEA peak.

The main problem with the method has been cross-contamination of samples and a lack of reproducibility. The MEA and any other polar compounds are being partially retained on the column even after the 10-minute hold at the maximum column temperature. A set of dilutions was injected onto the column with little impact on reproducibility past a dilution of 10:1. Figure 15 shows a non-degraded MEA sample injected 10 times after a sample spiked with HEEDA and oxazolidone.

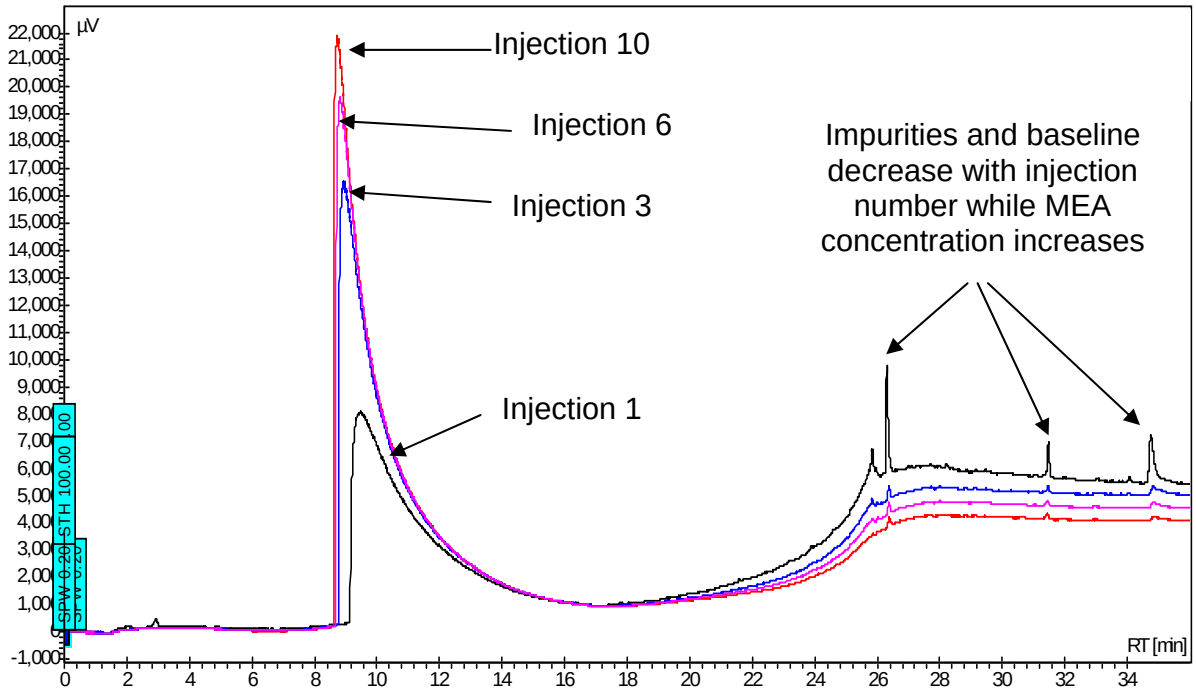

Figure 15. Undegraded MEA sample injected 10 times

From figure 15 you can see that with each subsequent injection, the MEA peak continues to grow, the impurity peaks get smaller, and the baseline shifts downward for the high temperature hold.

The method was modified with a longer hold time at the maximum temperature in order to elute any MEA that might remain on the column and by adding intermittent column rinses with DI water. This did not help much with the retention problem described above and did not alleviate the tailing. As a result of these problems a switch to a different column was in order, so we switched to a nonpolar column made by Agilent, the HP-5. The degradation samples for the 3, 5, and 8 week periods were injected on this column along with the MEA samples spiked with HEEDA and Oxazolidone. Figure 16 below shows the injection for the 3 week degraded sample.

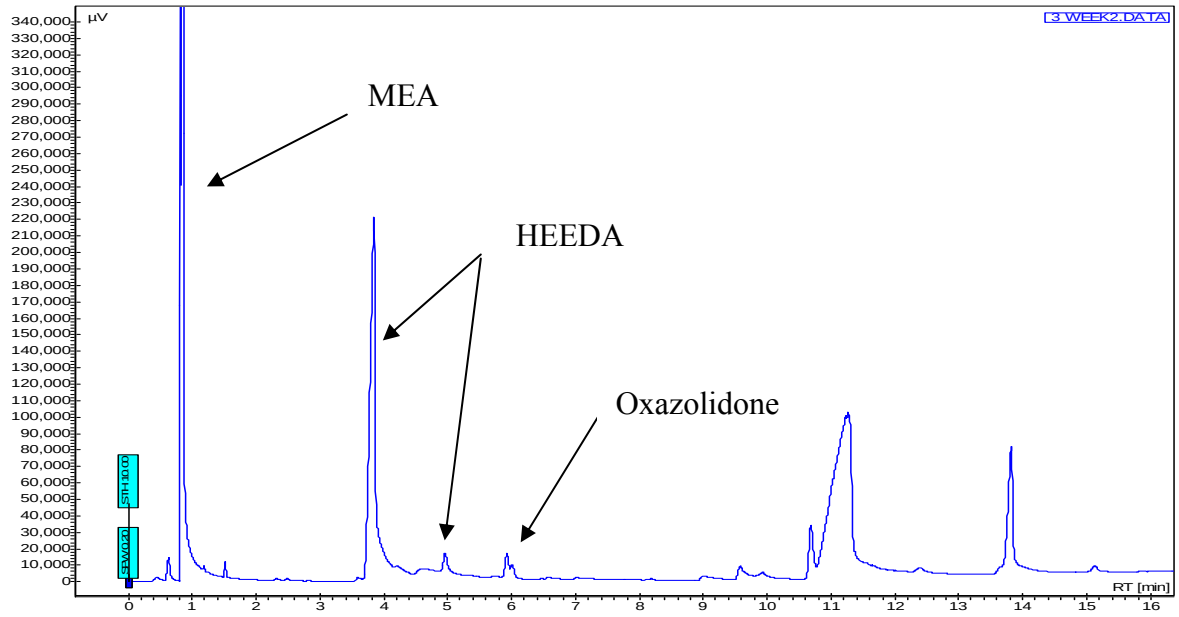

Figure 16. MEA degraded at 150°C for 3 weeks on HP-5 GC column

As you can see in Figure 16, the MEA peak does not tail into the subsequent impurity peaks. This column does not seem to retain the analytes as strongly and as a result there were no problems with column retention between samples. The one problem with this method is that the MEA elutes at roughly column dead time. This means that any nonretained species would coelute with the MEA making it difficult to say with certainty that the MEA peak was not masking potential impurities.

MEA losses were then estimated based on total MEA area counts for the time 0, 2, 3, 5, and 8 week samples. Figure 17 shows the total MEA area counts over time.

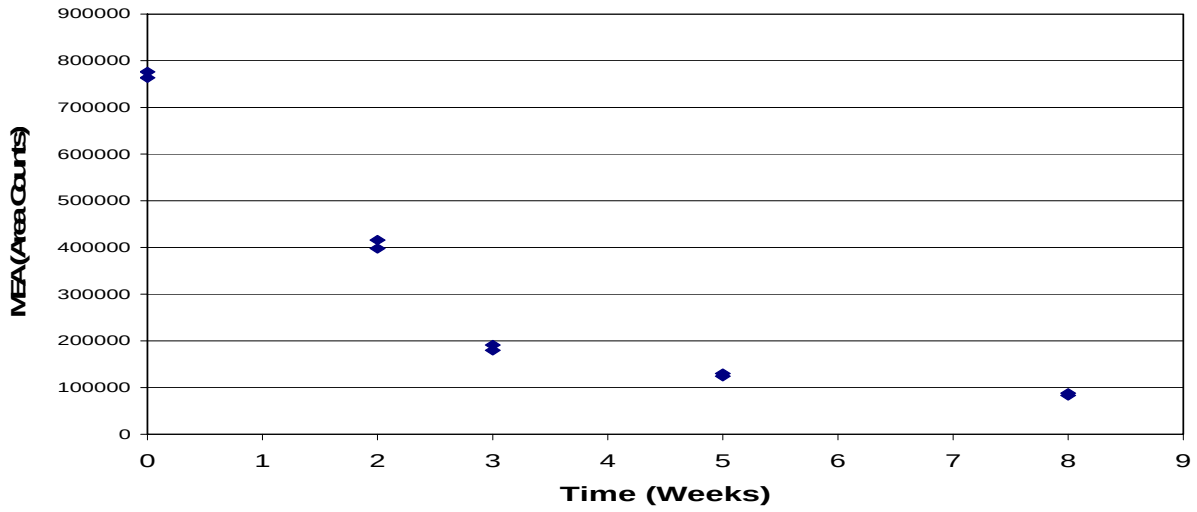

Figure 17. MEA losses at 150°C over an 8 week period. 30 wt % MEA, 0.4 moles CO_2/mole MEA

As you can see from Figure 17, the loss mechanism is an exponential decay with 75% degradation after just 3 weeks at 150°C. The amount of oxazolidone and HEEDA increased from the week 1 to week 3 samples, but actually decreased in the week 5 and 8 samples. Since the oxazolidone is in equilibrium with the amount of MEA carbamate present, it would make sense that it would decrease as the amount of available MEA decreased. The HEEDA would also decrease since it would further polymerize to higher molecular weight components and would be made at a slower rate due to the disappearance of oxazolidone.

Low Temperature Experiments

A set of 45 2ml sample bombs were constructed and placed in an oven at various amine concentrations and loadings and placed in an oven at 100°C for varying amounts of time. A set of the bombs were removed at 1 and 2 weeks time with additional times of 4, 6, and 8 weeks to be completed after the period covered by this report.

Little degradation has occurred over the first two weeks. Using the HP-5 column the total degradation of week 1 and week 2 samples versus the time 0 samples shows 0.3% and 2.3% MEA losses respectively which both fall within 1 standard deviation of the experimental results. More conclusive results should come with the longer hold times.

Future Work

Further method development will be pursued to obtain more reliable results with the INNOWAX column as a secondary GC method. A rinse with IPA to reduce the functionality of the column has been suggested as a possible solution to the tailing and retention. A HPLC method is also being pursued as an alternative to the GC method currently under development. This will focus on using hydrophilic interaction chromatography (HILIC) to separate the species. Since amines are highly polar in nature, this method should prove advantageous as it has been used to separate proteins and other highly polar analytes with success.

Subtask 3.4 – Amine Volatility

by Marcus Hilliard

(supported by the Industrial Associates Program)

Reagents

Sample solutions using the piperazine (PZ) and ultra pure deionized water (H_2O) from Acros Organics and the Department of Chemical Engineering at the University of Texas at Austin, respectively, were prepared without further purification. Carbon dioxide (CO_2) and nitrogen (N_2) gasses were obtained from Matheson Tri-Gas and the Cryogenics Laboratory at the University of Texas at a purity of 99.99 mol% and 99.0 mol%, respectively.

Experimental Methods

Tests were conducted in the stirred reactor system, documented in a previous report, using N_2 dilution as shown in Figure 18. The apparatus was designed to operate at atmospheric pressure and temperatures up to 70°C.

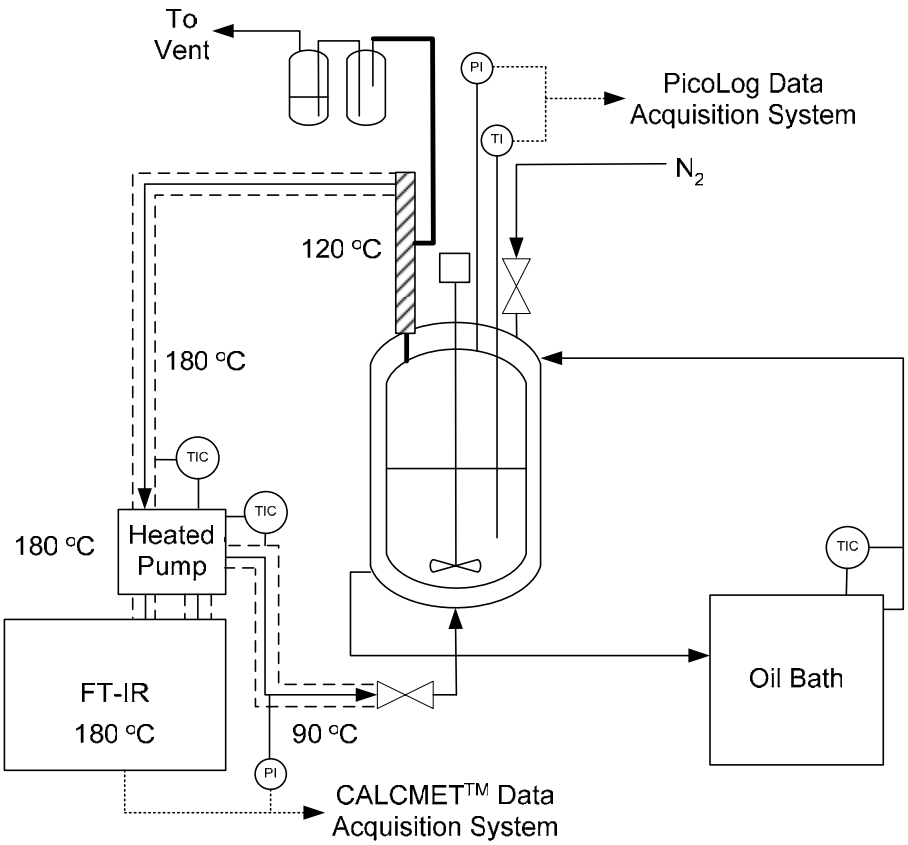

Figure 18. Process Flow Diagram for Vapor Phase Speciation Experiments

Results

Figure 19 compares CO_2 solubility measurements from this work to predictions from Hilliard (2002) and Ermatchkov, et al. (2006) for a 2 m PZ solution at 40 and 60°C. Previous model predictions and experimental data from the literature seem to agree with the new experimental data from this study over the range in loadings.

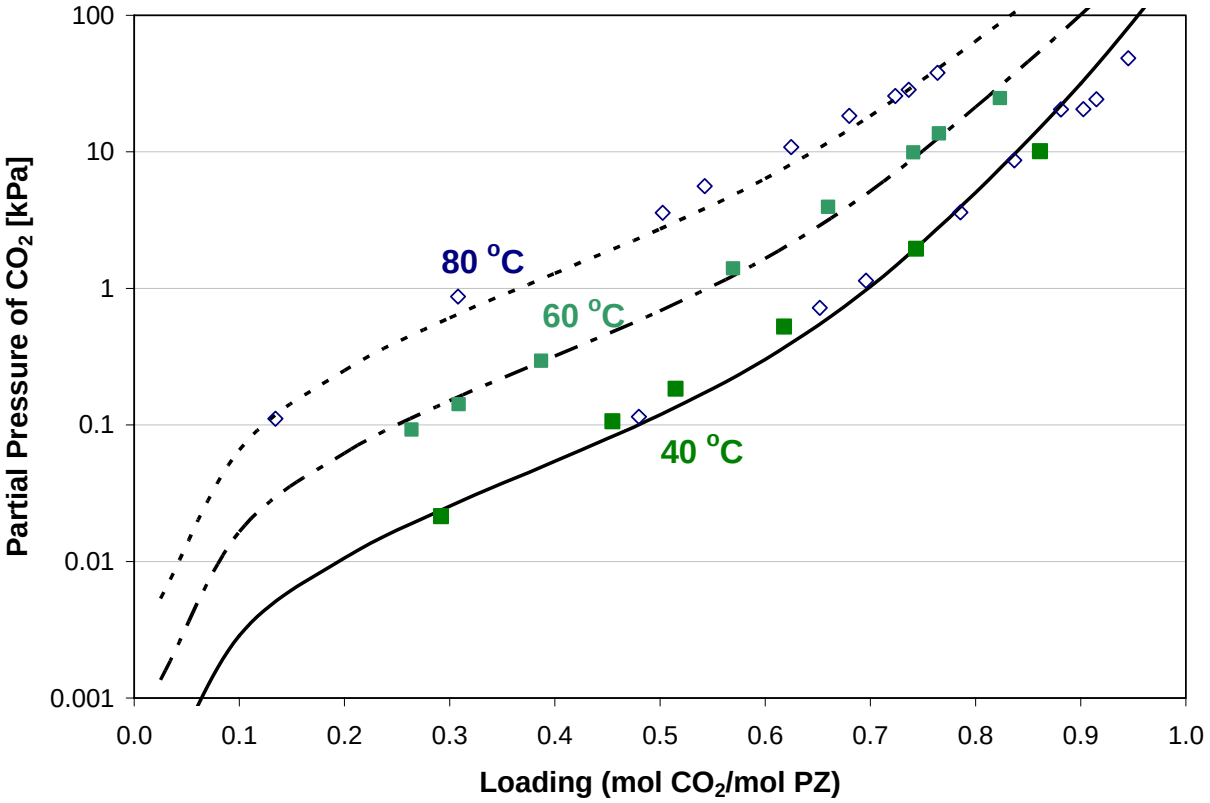

Figure 19. Comparison of CO_2 solubility in 2 m PZ from this work and Ermatchkov et al. (2006) to predictions from Hilliard (2005) at 40, 60, and 80°C

Future work

Work will continue to quantify the CO_2 solubility and amine volatility for 0.9, 2.5, and 5 m PZ.

Conclusions

Our research has been able to benchmark our experimental apparatus for measurement of CO_2 solubility against literature data. We are now confident in our approach and will continue our efforts in this area.

Subtask 4.1a – Reclaiming by crystallization – potassium sulfate

by Qing Xu

(supported by the Industrial Associates Program)

Introduction

One side reaction in CO_2 capture when using MEA is the generation of sulfate from SO_2. This sulfate has to be removed so that the MEA solution can be reused for CO_2 capture. Potassium compounds can be used in the removal of sulfate. In order to determine how best to accomplish this, the solubility of potassium sulfate was measured with variable MEA concentration and CO_2 loading.

Experimental

Method 1

The first experimental method was used by a group of undergraduate students as a special project in a senior laboratory course (Sachde and Sivaram, Summer 2006).

Solutions were gravimetrically prepared with 3, 7, 11.4, and 15 m MEA (moles amine/kg water). Then 10ml of MEA solution was mixed with 1.5g K_2SO_4 and agitated in a water bath for about 48 hours. Four temperatures (25, 40, 60, and 80ºC) were chosen within the operating range of the absorption-stripping system.

Undissolved solids were collected using vacuum filtration, dried, and weighed with a balance. The solids dissolved in the solution sample were also dried and weighed to determine residual K_2SO_4 to reduce error. The filtration process was performed quickly to prevent the filtrate from cooling down so that no K_2SO_4 would precipitate out of solution.

Method 2

The second experimental method was used by a group of undergraduate students as a special project in a senior laboratory course (Abesamis et al., Fall 2006).

7 m MEA was prepared gravimetrically as a stock solution. 100g of this solution was agitated with a stir bar. Solid K_2SO_4 was added to the system in 0.1g increments. The conductivity of the solution was measured with each addition. Additions were continued until the solution was saturated. Then an excess of K_2SO_4 was added to the solution and the final conductivity was measured. A correlation of conductivity and K_2SO_4 concentration was developed from the data collected before saturation and the concentration at saturation was calculated with the correlation from the final measured conductivity.

In modifications of this procedure, KOH or H_2SO_4 was added to the solution before the additions of K_2SO_4.

A water bath was used to conduct these experiments at 45ºC and 60ºC.

Method 3, CO_2 loaded

This method was used to measure loaded solutions.

A bubbler was used to add CO_2 to stock solution of 7 m MEA. The amount of CO_2 added to the solution was weighed with a balance. In this experiment, a sufficient amount of CO_2 was added to form a 2.8 molal CO_2 solution. Another way to prepare CO_2 loading solution is by adding $KHCO_3$ to form 2.8 molal $KHCO_3$ solutions.

50g of the loaded solution was agitated by a stir bar during the following process. 0.2-0.4g K_2SO_4 was sequentially added to the system and conductivity was measured with each addition until the solution was saturated. Then an excess of K_2SO_4 was added to the solution and the final conductivity was recorded. Conductivity was correlated with K_2SO_4 concentration and extrapolated to obtain the K_2SO_4 saturation concentration.

The experiments were all carried out at room temperature.

Model Formulation

A model of ln(K_{sp}), depending on $\frac{1}{T}$, I^a, and the concentration of MEA, was developed.

'I' is the iron strength of the solution and 'a' is its exponent. Linear models were developed, where different exponents (range from 0 to 0.6) were used. By comparing the error and coefficients of determination from each model, the proper exponent, a=0.1, was determined.

Model 1

$$\ln Ksp = 17.29 I^{0.1} - 0.385[MEA] - \frac{1324.1}{T} - 13.989$$

Theory

The Ksp (m^3) is given by:

$$Ksp = [K^+]^2[SO_4^{2-}]$$

For MEA solution with loaded CO_2 and K_2SO_4, the ionic strength (m) is given by:

$$I = \frac{1}{2}([K^+] + 4 \times [SO_4^{2-}] + [MEACOO^-] + [MEAH^+])$$

The coefficient of determination, R^2, was 0.975.

The data from which the model was developed are listed in Table 18:

Table 18. Conditions giving solutions saturated to K_2SO_4

T ( )	[MEA](m)	CO_2(m)	KOH(m)	H_2SO_4(m)	I (m)	Ksp(m^3)		
						meas	calc	calc/meas
Sachde and Sivaram, 2006								
25	7	0	0.25	0.125	0.375	7.8E-03	4.3E-03	5.5E-01
25	11.4	0	0.08	0.04	0.121	2.6E-04	1.5E-04	5.8E-01
25	15	0	0.097	0.049	0.146	4.6E-04	4.8E-05	1.0E-01
40	3	0	0.601	0.301	0.902	1.1E-01	1.0E-01	9.6E-01
40	7	0	0.239	0.119	0.358	6.8E-03	4.9E-03	7.3E-01
40	11.4	0	0.083	0.042	0.125	2.9E-04	1.9E-04	6.6E-01
40	15	0	0.016	0.008	0.024	2.0E-06	5.6E-06	2.8E+00
60	3	0	0.733	0.367	1.1	2.0E-01	1.9E-01	9.6E-01
60	7	0	0.302	0.151	0.452	1.4E-02	9.2E-03	6.7E-01
60	11.4	0	0.128	0.064	0.192	1.0E-03	4.6E-04	4.3E-01
60	15	0	0.017	0.008	0.025	2.3E-06	7.6E-06	3.3E+00
80	3	0	0.692	0.346	1.038	1.7E-01	2.1E-01	1.3E+00
80	7	0	0.305	0.152	0.457	1.4E-02	1.2E-02	8.3E-01
80	11.4	0	0.129	0.065	0.194	1.1E-03	5.8E-04	5.4E-01
80	15	0	0.022	0.011	0.033	5.3E-06	1.3E-05	2.5E+00
Abesamis et al., 2006								
25	7	0	0.112	0.056	0.168	7.0E-04	1.3E-03	1.8E+00
25	7	0	0.183	0.035	0.162	1.2E-03	1.2E-03	1.0E+00
25	7	0	0.112	0.112	0.336	1.4E-03	3.6E-03	2.6E+00
This work (CO_2 loaded)								
23.45	7	2.8	0.614	0.307	3.721	1.2E-01	2.4E-01	2.1E+00
22.25	7	2.8	0.597	0.299	3.696	1.1E-01	2.3E-01	2.2E+00
22.6	7	2.8	2.79	0	2.8	0.0E+00	1.4E-01	
23.8	7	2.8	0.836	0.218	3.455	1.5E-01	2.1E-01	1.4E+00
CRC Handbook of Chemistry and Physics, 87th edition								
25	0	0	1.375	0.688	2.063	1.3E+00	1.2E+00	9.0E-01
30	0	0	1.477	0.738	2.215	1.6E+00	1.4E+00	8.9E-01
40	0	0	1.7	0.85	2.55	2.5E+00	2.2E+00	8.8E-01
50	0	0	1.899	0.95	2.849	3.4E+00	3.0E+00	8.9E-01
60	0	0	2.105	1.053	3.158	4.7E+00	4.2E+00	9.0E-01
70	0	0	2.301	1.15	3.451	6.1E+00	5.6E+00	9.2E-01
80	0	0	2.468	1.234	3.703	7.5E+00	7.2E+00	9.5E-01

The error dependence on ionic strength and MEA concentration is shown in Figure 20 and Figure 21, respectively:

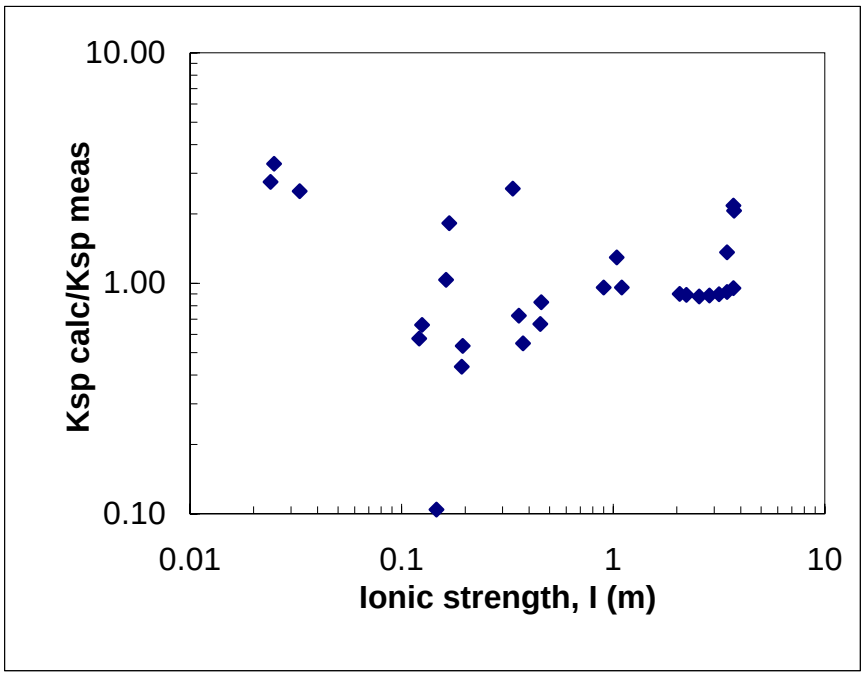

Figure 20. Error in model prediction of K_2SO_4 solubility in MEA solutions

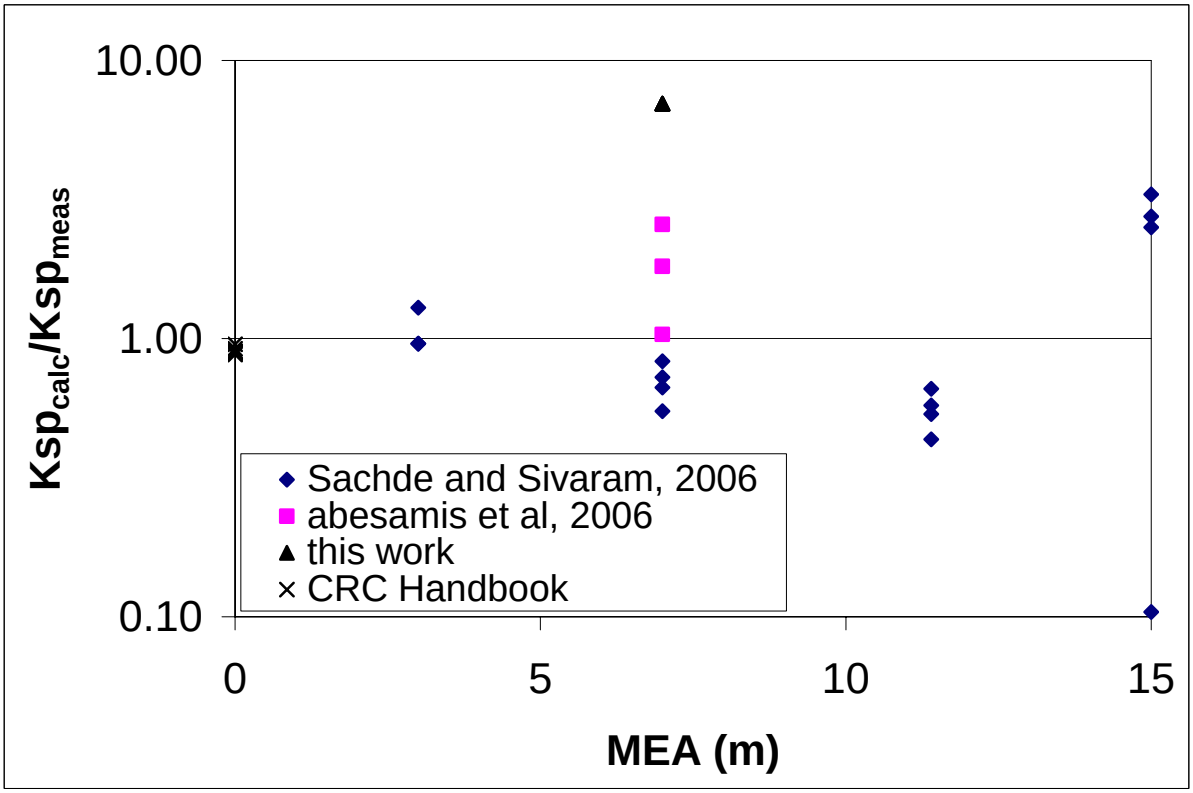

Figure 21. Comparison calculated and measured K_2SO_4 solubility as a function of MEA concentration

Results and Discussion

Effect of I on Ksp.

From the model:

$$\ln Ksp = 17.29 I^{0.1} - 0.385[MEA] - \frac{1324.1}{T} - 13.989$$

According to the data at: [MEA]=7 m, T=23ºC, Ksp dependence on $I^{0.1}$ can be seen from figure 3 as below, where Ksp is in log scale:

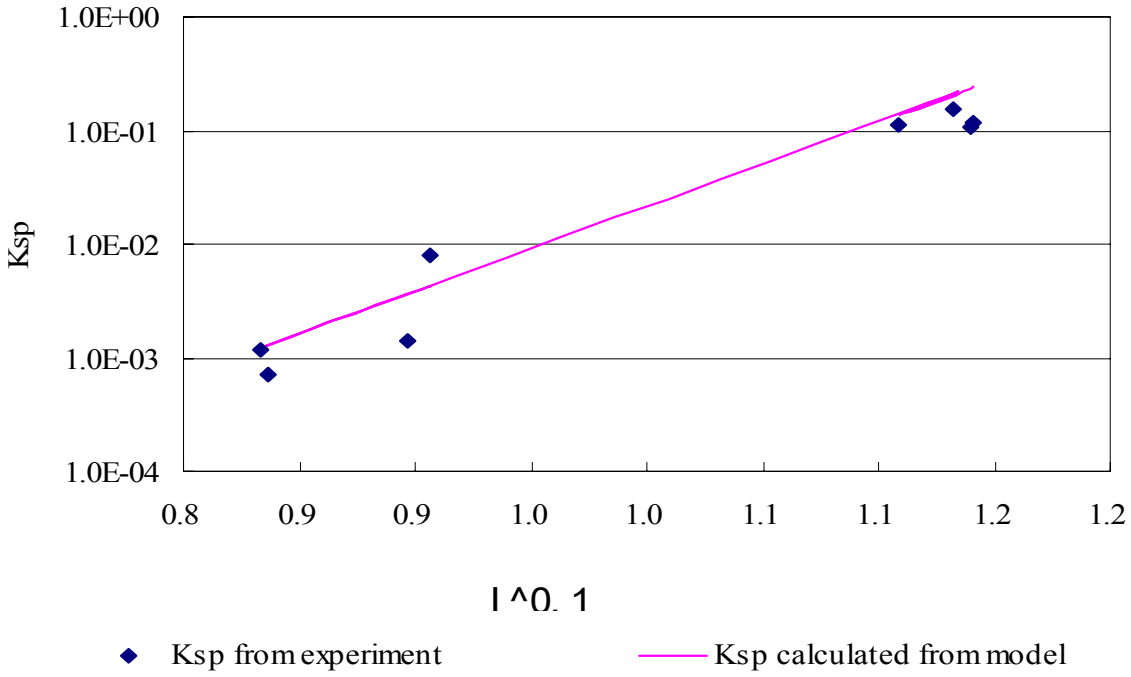

Figure 22: The solubility of K_2SO_4 in 7 m MEA at 23°C

Girard (1885) gives the solubility of potassium sulfate in aqueous ammonia. The more NH_3 in solvent, the less solubility of K_2SO_4 will be. The solubility increases as temperature increases. At 20ºC, the data is in table 2:

Table 19. Solubility of potassium sulfate in aqueous ammonia solutions at 20ºC

Gms. NH_3 per 100 cc solution	0	5.2	6.086	15.37	24.69	31.02
Gms. K_2SO_4 per 100 cc solution	10.80	4.52	4.10	0.83	0.14	0.04
Concentration of NH_3 in molal	0.00	3.39	3.99	10.79	19.32	26.47
Concentration of K_2SO_4 in molal	0.696	0.288	0.262	0.057	0.011	0.0033
I (ionic strength)	2.088	0.863	0.787	0.171	0.032	0.010
Ln(Ksp(K_2SO_4))	0.30	-2.35	-2.63	-7.21	-12.23	-15.72
Ln(Ksp) calculated with the model*	0.10	-2.78	-3.16	-8.17	-13.69	-17.79
Error	0.82	0.65	0.59	0.38	0.23	0.13

*Under the same I, T, and use the molal concentration of NH_3 instead of [MEA].

Figure 23 compares the measured solubility of K_2SO_4 in ammonia solution with that predicted by the model developed for MEA solutions:

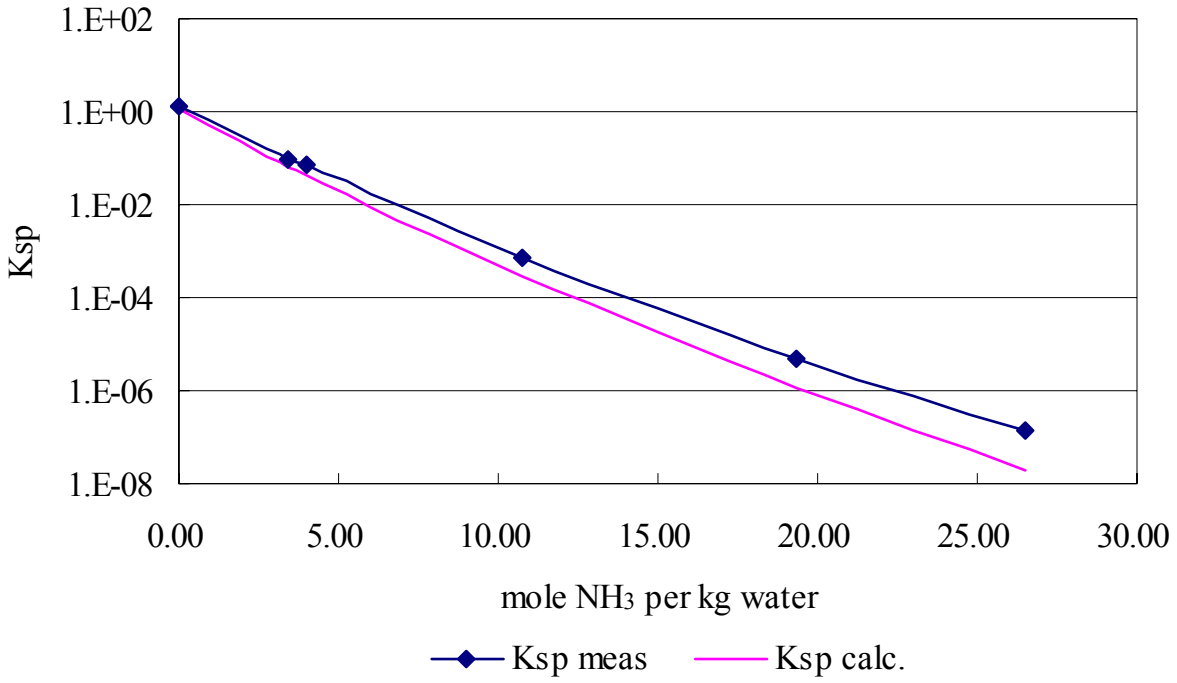

Figure 23. Solubility of potassium sulfate in aqueous ammonia solutions at 20°C

Our model does a very good job of predicting K_2SO_4 solubility in NH_3 solution when [NH_3] is in low concentration.

Conclusions

A model of the solubility of potassium sulfate in MEA solution has been developed and tested by the data from both experiments and references. It can fit the data from experiment well, and can roughly fit the data of potassium sulfate in NH_3 solution in some concentration ranges, which may help in the prediction of K_2SO_4 solubility in MEA solution. In 7 m MEA solution, with no extra K^+ or SO_4^{2-} at 25ºC, Ksp of K_2SO_4 can be about 0.004m^3 without CO_2 and 0.23m^3 with CO_2 loaded.

Future work

Additional data will be obtained on K_2SO_4 solubility in loaded MEA solution over a broader range of temperature and MEA concentration.

Task 5 – Corrosion

Subtask 5.1 – Corrosion in base solution compared to MEA

by Amornvadee (Amy) Veawab, University of Regina

(supported by subcontract)

Introduction

The carbon dioxide (CO_2) absorption process using aqueous chemical solutions is subject to a number of operational difficulties, of which the most severe is corrosion of process equipment and solvent degradation. Corrosion problems have been receiving a great deal of attention because they have substantial impacts on a plant's economy, especially in terms of unplanned downtime, production losses, reduced equipment life, and extra expenditure for restoring the corroded equipment and for treatment systems initiated to mitigate the corrosion. The corrosion problems also prevent the absorption process from achieving energy efficient operations.

The aqueous solution of blended potassium carbonate and piperazine has been demonstrated to be a promising solvent for CO_2 capture from coal-fired power plant flue gas due to its capture performance and energy efficiency. It is our goal to explore further the promise of this solvent in an aspect of the potential operational problems. This project focuses on the investigation of corrosion of materials during CO_2 absorption and solvent regeneration in the presence and absence of solvent degradation products and chemical additives including oxidative inhibitors and corrosion inhibitors.

The research involves comprehensive literature review on corrosion in the CO_2 absorption process using potassium carbonate and piperazine, and experimental evaluations in the following sequences.

Task 1: Evaluation of corrosion in base solution (the blended potassium carbonate and piperazine) against the corrosion in an aqueous solution of monoethanolamine (MEA).

Task 2: Evaluation of corrosion in base solution containing degradation products.

Task 3: Evaluation of corrosion in base solution containing degradation products and oxidative inhibitors.

Task 4: Evaluation of inhibition performance of corrosion inhibitor in the presence of degradation products and oxidative inhibitors.

Based on our discussion with Dr. Rochelle, we would like to expand our project to cover the corrosion study in both K_2CO_3-piperazine and MEA-piperazine since MEA-piperazine is another promising piperazine-based solvent for cost-effective CO_2 capture. The original tasks for K_2CO_3-MEA will be kept minimum, and the tasks with similar objectives will be carried out for MEA-piperazine system.

Experimental

Over the past three months, we have been conducting a series of short-term electrochemical corrosion experiments under various conditions to obtain the corrosion rate of carbon steel and gain understanding of corrosion behavior in aqueous solutions of blended MEA-piperazine. Results and discussion are provided below.

1. Effect of thiosulfate

Electrochemical corrosion experiments were carried out in aqueous solutions of blended 5M MEA/1.2M piperazine containing 1 wt % ammonium thiosulfate and 0.20 mol/mol CO_2 loading at 80^{o}C. The results in Figures 24-25 show that thiosulfate causes a small increment in corrosion rate of carbon steel in both deaereated and aerated systems. Its corrosion rate is the lowest compared to the heat-stable salts tested previously (i.e. oxalate, formate and acetate). It is apparent from cyclic polarization curves (Figures 26-27) that thiosulfate does not induce passive

film under the test condition. Corrosion takes place in the active state of carbon steel and produces iron carbonate ($FeCO_3$), which is thermodynamically stable as shown in Pourbaix diagrams (Figures 28-29). No pitting tendency was found.

2. Effect of copper carbonate ($CuCO_3$)

The inhibition performance of $CuCO_3$ was examined in aqueous solutions of blended 5M MEA/1.2M piperazine containing 0.20 mol/mol CO_2 loading at 80°C. The presence of oxygen plays an important role in inhibition performance of $CuCO_3$. As shown in Figures 30-31, the increase in oxygen content in gas from 0 to 10% leads to the decrease in corrosion rate. This suggests that $CuCO_3$ performs more effectively in the presence of dissolved oxygen. This is perhaps due to the nature of passive film formed on the metal surface. According to the Pourbaix diagram (Figures 32-33), it is thermodynamically possible that the passive film in the absence of oxygen is magnetite (Fe_3O_4) while that in the presence of oxygen is hematite (γ-Fe_2O_3). The hematite has superior inhibition to the magnetite. Their film formation reactions are shown below:

$$3Fe + 4H_2O \rightarrow Fe_3O_4 + 4H_2 \quad (1)$$

$$2Fe_3O_4 + H_2O \rightarrow 3Fe_2O_3 + H_2 \quad (2)$$

Figures 34-36 illustrate typical polarization curves of carbon steel immersed in the solutions inhibited by $CuCO_3$. It is apparent that $CuCO_3$ is an anodic corrosion inhibitor. $CuCO_3$ inhibits corrosion by shifting the corrosion potential of metal from an active to a passive state where a passive film is formed on the metal surface. The passive film acts as a separator of metal surface and solution, thus retarding the diffusion of Fe^{2+} and electrons from the metal surface to the solution. As a result, the corrosion reactions proceed at a slower rate. It should however be noted that $CuCO_3$ with a concentration of 50 ppm in the absence of oxygen does not induce such passive film (Figure 37). The carbon steel is thus in an active state where corrosion takes place. The cyclic polarization curves also exhibit positive hysteresis, indicating that $CuCO_3$ tends to induce pitting.

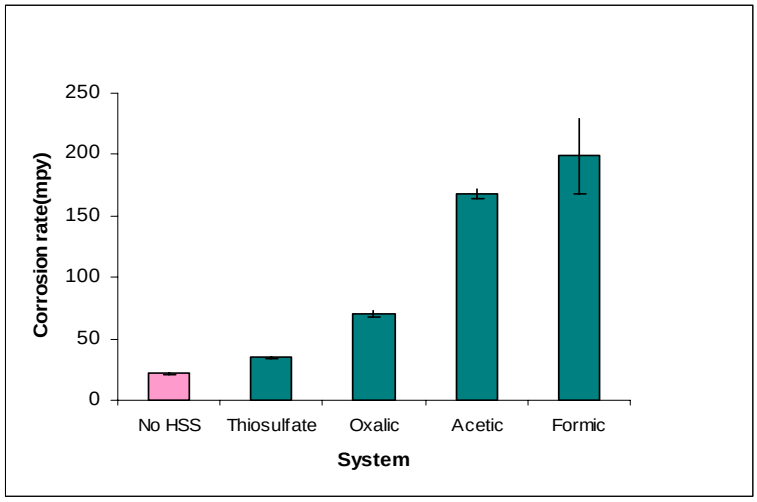

Figure 24. Corrosion rates of carbon steel in 5M MEA-1.2M PZ containing 1 wt % heat-stable salt and 0.20 mol/mol CO_2 loading

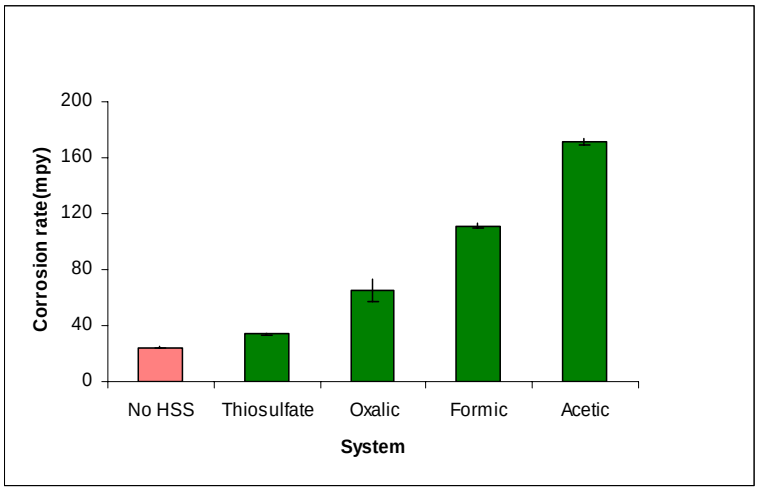

Figure 25. Corrosion rates of carbon steel in 5M MEA-1.2M PZ containing 1 wt % heat-stable salt and 0.20 mol/mol CO_2 loading and with 10% oxygen

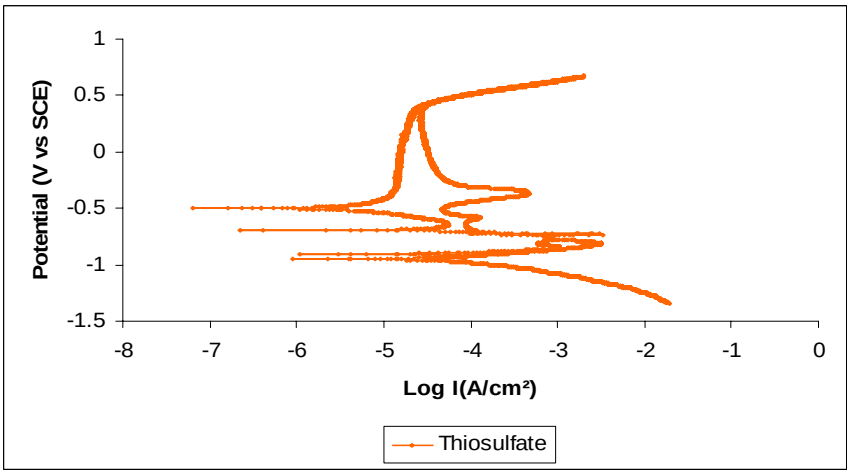

Figure 26. Cyclic polarization curve of carbon steel in 5M MEA-1.2M PZ containing 1 wt % ammonium thiosulfate and 0.20 mol/mol CO_2 loading

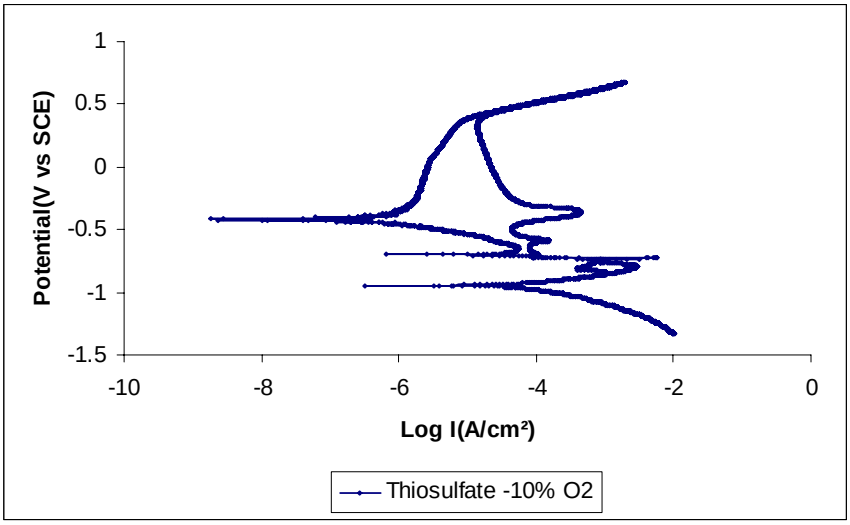

Figure 27. Cyclic polarization curve of carbon steel in 5M MEA-1.2M PZ containing 1 wt % ammonium thiosulfate and 0.20 mol/mol CO_2 loading with 10% oxygen

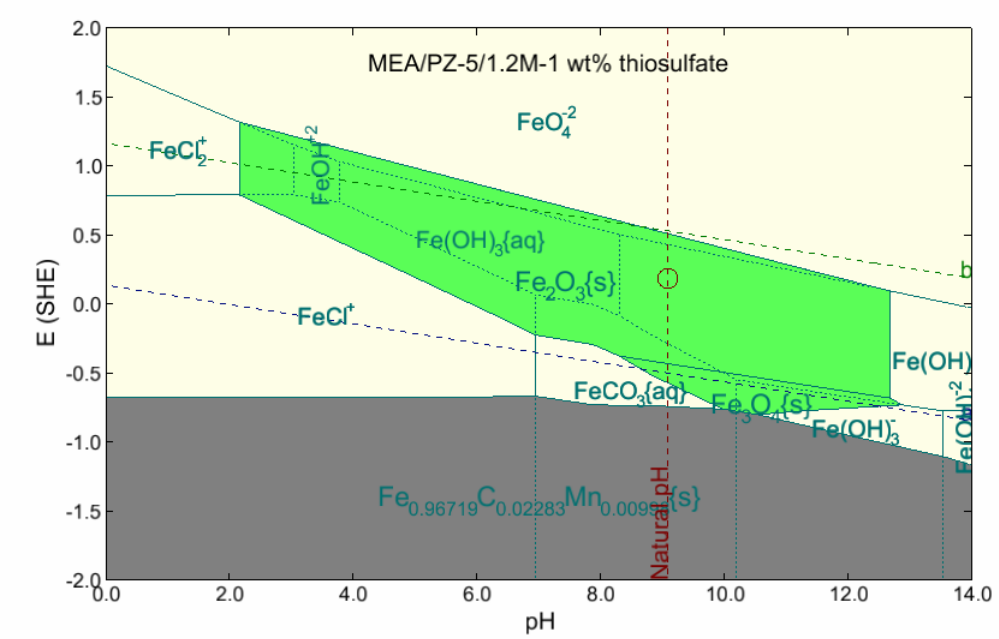

Figure 28. Pourbaix diagram for 5M MEA/1.2M PZ containing 1 wt % ammonium thiosulfate and 0.20 mol/mol CO2 loading at 80oC

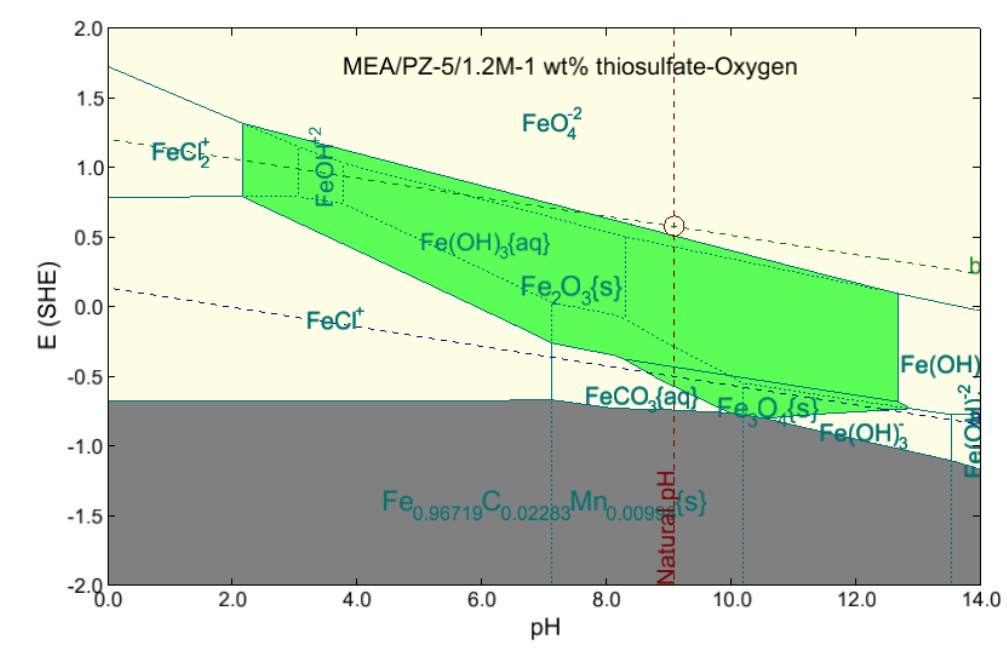

Figure 29. Pourbaix diagram for 5M MEA/1.2M PZ containing 1 wt % ammonium thiosulfate and 0.20 mol/mol CO_2 loading at 80°C with 10% oxygen

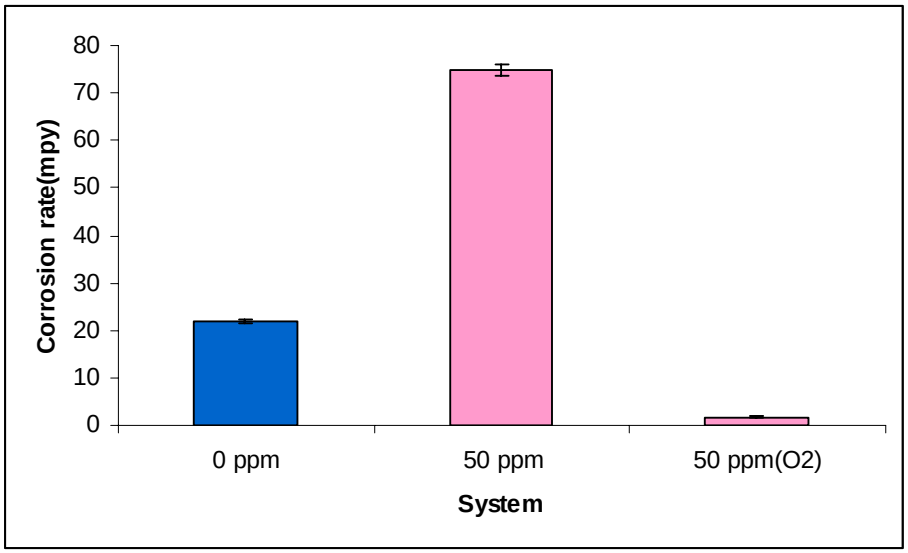

Figure 30. Corrosion rates of carbon steel in 5M MEA-1.2M PZ containing 50 ppm $CuCO_3$ and 0.20 mol/mol CO_2 loading at 80°C

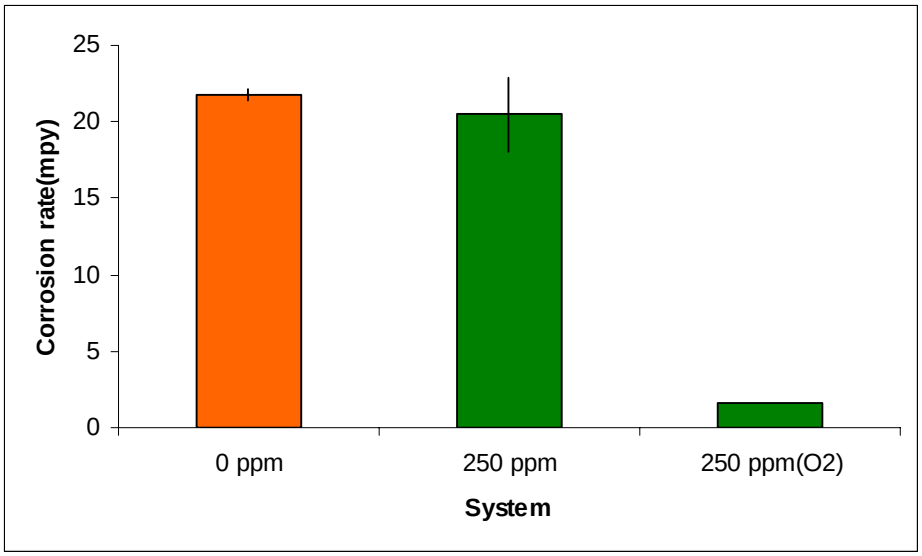

Figure 31. Corrosion rates of carbon steel in 5M MEA-1.2M PZ containing 250 ppm $CuCO_3$ and 0.20 mol/mol CO_2 loading at 80°C

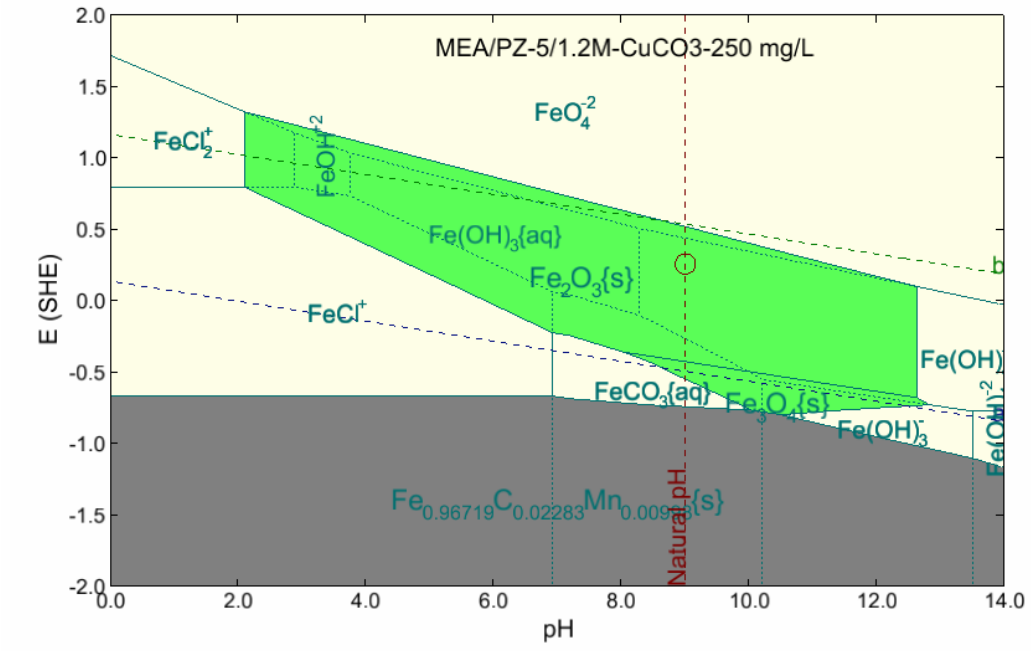

Figure 32. Pourbaix diagram for 5M MEA/1.2M PZ containing 250 ppm $CuCO_3$ and 0.20 mol/mol CO_2 loading at 80°C

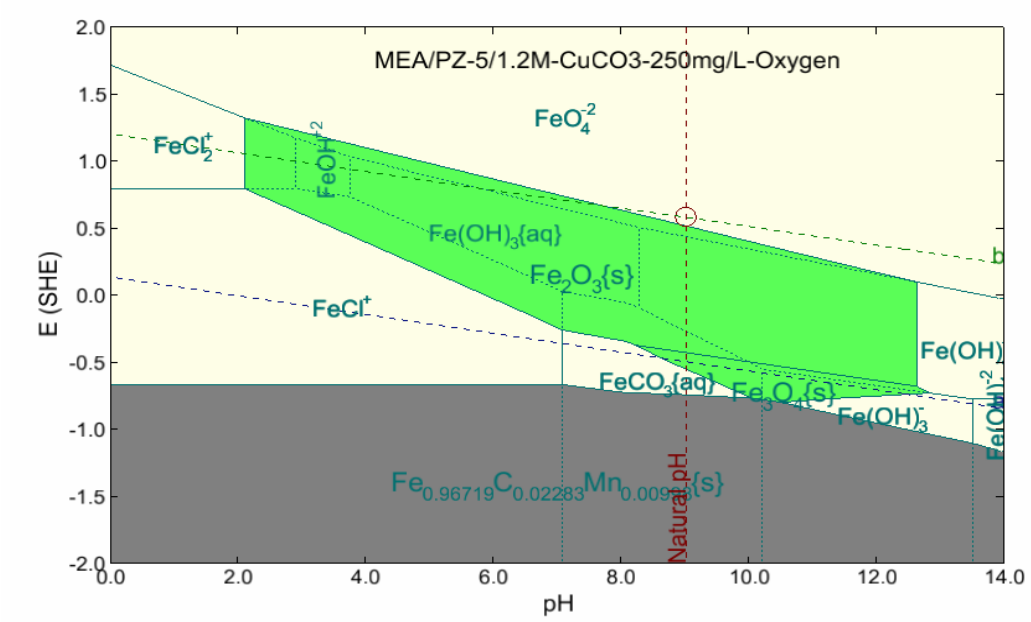

Figure 33. Pourbaix diagram for 5M MEA/1.2M PZ containing 250 ppm $CuCO_3$ and 0.20 mol/mol CO_2 loading at 80°C with 10% oxygen

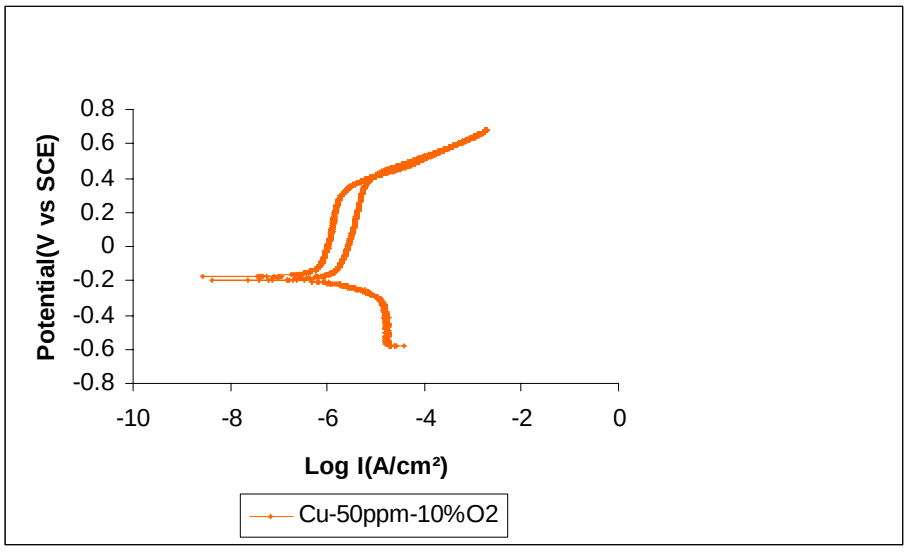

Figure 34. Cyclic polarization curve of carbon steel in 5M MEA-1.2M PZ containing 50 ppm CuCO3 and 0.20 mol/mol CO2 loading at 80oC with 10% oxygen

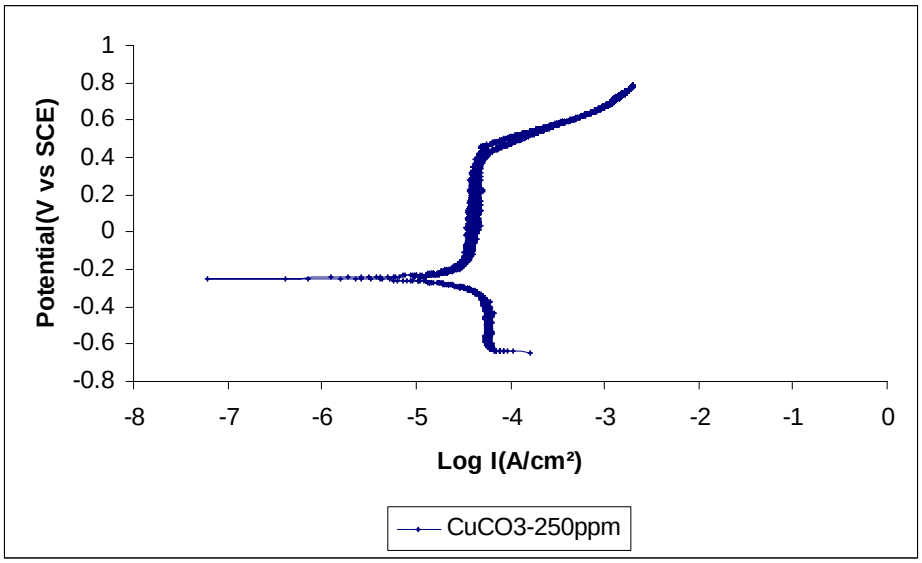

Figure 35. Cyclic polarization curve of carbon steel in 5M MEA-1.2M PZ containing 250 ppm $CuCO_3$ and 0.20 mol/mol CO_2 loading at 80°C

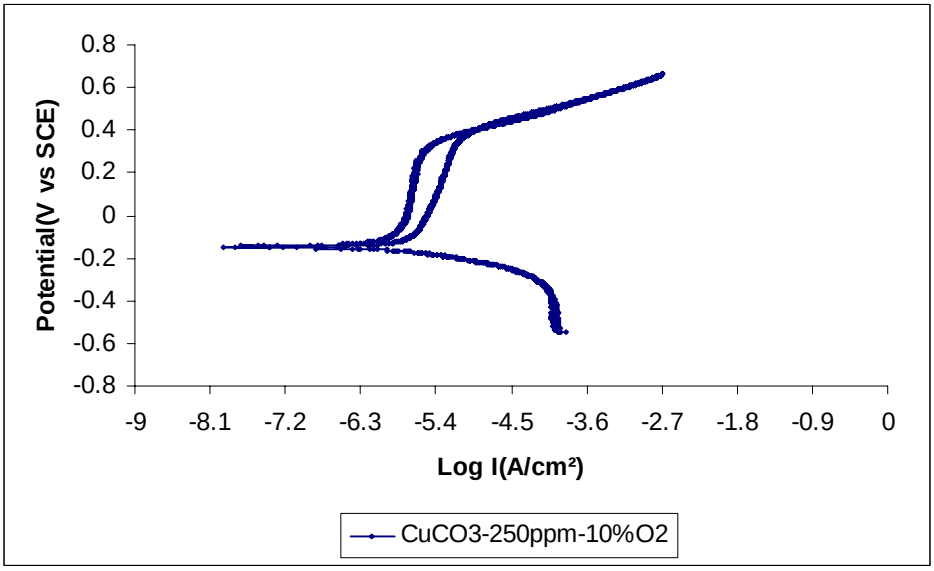

Figure 36. Cyclic polarization curve of carbon steel in 5M MEA-1.2M PZ containing 250 ppm CuCO3 and 0.20 mol/mol CO2 loading at 80oC with 10% oxygen

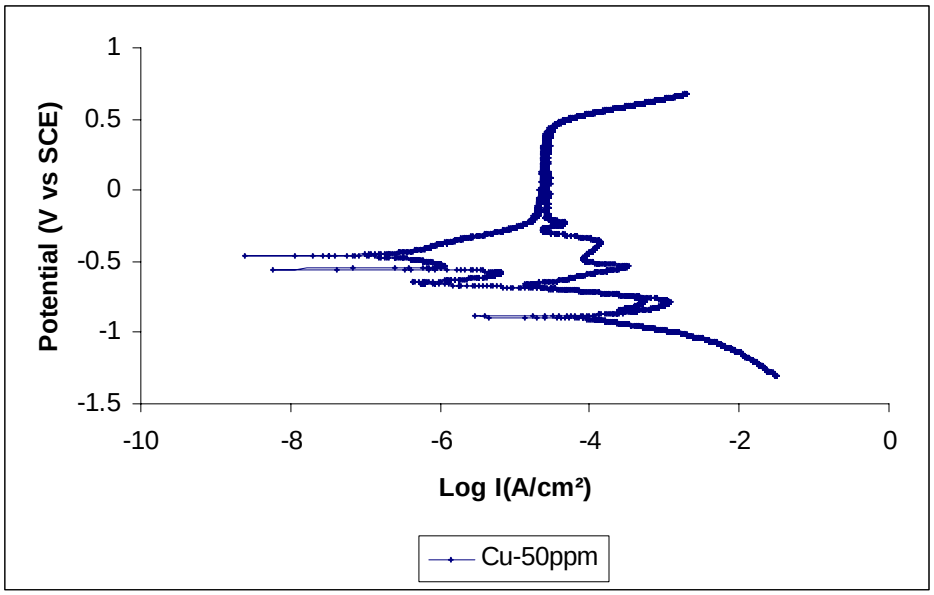

Figure 37. Cyclic polarization curve of carbon steel in 5M MEA-1.2M PZ containing 50 ppm $CuCO_3$ and 0.20 mol/mol CO_2 loading at 80°C

References

Abesamis, A, B. Bayer, and R. Hai, "Crystallization of Potassium Sulfate," ChE 264 special project, University of Texas, Austin (Fall 2006).

Bishnoi, S. "Carbon Dioxide Absorption and solution equilibrium in piperazine-activated methyldiethanolamine." PhD Dissertation, University of Texas, Austin (2000).

Blezard, Michael, and Glyn R. Jones, "Nitrosamine inhibition," U. S. Patent Application No. 5,223,644 (1993).

Calle, Emilio, Julio Casado, Jose L. Cinos, Francisco J. Garcia Mateos, and Manuel Tostado, "Formation of nitrosamines in alkaline conditions: a kinetic study of the nitrosation of linear and cyclic secondary amines by nitroalkanes," *J. Chem. Soc*, Perkin II, 1559-1564 (1992).

Challis, B. C., and J. A. Challis, "*N*-nitrosamines and *N*-nitrosoimines, *The chemistry of amino, nitroso and nitro compounds and their derivatives*," Supplement F, Part 2, edited by S. Patai, Wiley, New York, 1151-1223 (1982).

Challis, B. C. and S. A. Kyrtopoulos, "The Chemistry of Nitroso-compounds. Part 11. Nitrosation of amines by the two-phase interaction of amine in solution with gaseous oxides of nitrogen," *J. Chem. Soc*., Perkin I (1979).

Chen, C. C., and L. B. Evans, "A local composition model for the excess Gibbs energy of aqueous electrolyte systems," *AIChE J.*, **32**(3), 444-454 (1986).

CRC Handbook of Chemistry and Physics, 87th edition, online, section 8-114, http://www.hbcpnetbase.com/articles/08_21_86.pdf

Cullinane, J. T., "Thermodynamics and Kinetics of aqueous piperazine with potassium carbonate for carbon dioxide absorption," PhD Dissertation, University of Texas, Austin (2005).

Dawodu, O. F., and A. Meisen, "Gas chromatographic analysis of alkanolamine solutions using capillary and packed columns," *J. Chromatog.*, **629**(2), 297-307 (1993).

Dawson, Brian A., and Robert C. Lawrence, "Analysis of piperazine drug formations for *N*-nitrosamines," *J. Assn. Off. Anal. Chem.*, **70**(5), 840-841 (1987).

Dionex IonPac CS17 *Analytical Column Product Manual*, Revision 03, May 2003. http://www1.dionex.com/en-us/webdocs/manuals/ic/31747-03_CS16_V19.pdf (Accessed January 2005).

Elespuru, R.K. and W. Lijinsky, "Mutagenicity of cyclic nitrosamines in *Escherichia coli* following activation with rat liver microsomes," *Cancer Research*, 4099-4101 (1976).

Freguia, S., and G. T. Rochelle, "Modeling of CO_2 Capture by Aqueous Monoethanolamine," *AIChE J.*, **49**(7), 1676-1686 (2003).

Girard, in William F. Linke, PhD Dissertation, "Solubilities, Inorganic and Metal-Organic Compounds K-Z," Volume II, American Cyanamid Co., Stamford, Conn. 301 (1885).

Goff, G. S., and G. T. Rochelle, "Monoethanolamine Degradation: O_2 Mass Transfer Effects under CO_2 Capture Conditions," *Ind. Eng. Chem. Res.*, **43**(20), 6400-6408 (2004).

Hilliard, M. D., "Thermodynamics of aqueous piperazine/potassium carbonate/carbon dioxide characterized by the electrolyte NRTL model with AspenPlus®," M.S. Thesis, University of Austin, Texas (2005).

Keefer, L.K., and P. P. Roller, "*N*-Nitrosation by Nitrite Ion in Neutral and Basic Medium," *Science*,**181**, 1245-1247 (1973).

Kirsch, Michael, Hans-Gert Korth, Reiner Sustmann, and Herbert De Groot, "Carbon Dioxide but Not Bicarbonate Inhibits *N*-Nitrosation of Secondary Amines. Evidence for Amine Carbamates as Protecting Entities," *Chem. Res. in Tox.*, **13**(6), 451-461 (2000).

Klein, R. G., "Calculations and measurements on the volatility of *N*-nitrosamines and their aqueous solutions," *Toxicology*, **23**(2-3), 135-147 (1982).

Linke, W. F., and A. Seidell, *Solubilities, Inorganic and Metal-Organic Compounds*, D. Van Nostrad, Princeton, NJ (1958).

Littel, R. J., "Selective Carbonyl Sulfide Removal in Acid Gas Treating Processes," PhD Dissertation, Twente University (1991).

Love, L. A., W. Lijinsky, L. Keefer, and H. Garcia, "Chronic oral administration of 1-nitrosopiperazine in high doses to MRC rats," *Z. Krebsforsch*., 69-73 (1977).

Lovejoy, D. J., and A. J. Vosper, Part VI. "The Reaction of Dinitrogen Trioxide with Primary and Secondary Amines," *J. Chem. Soc.* (A), 2325-2328 (1968).

Mock, B., L. B. Evans, and C. C. Chen, "Thermodynamic representation of phase equilibria of mixed-solvent electrolyte systems," *AIChE J.*, **32**(10), 1655-1664 (1986).

Onda, K., H. Takeuchi, and Y. Okumoto, "Mass transfer coefficients between gas and liquid phases in packed columns," *J. Chem. Eng. Japan*, **I**(1), 56-62 (1968).

Oyenekan, B. A., and G. T. Rochelle, "Alternative Stripper Flow Schemes for CO_2 Capture by Aqueous Amines," University of Texas, Austin (2006a).

Oyenekan, B. A., and G. T. Rochelle, "Rate Modeling of CO_2 Stripping from Potassium Carbonate promoted by Piperazine," University of Texas, Austin (2006b).

Oyenekan, B. A., and G. T. Rochelle, "Energy Performance of Stripper Configurations for CO_2 Capture by Aqueous Amines," *Ind. Eng. Chem. Res.*, **45**(8), 2457-2464 (2006).

Oyenekan, B. A., and G. T. Rochelle, "Alternative Stripper Configurations to Minimize Energy for CO_2 Capture," In 8th International Conference on Greenhouse Gas Control Technologies, Trondheim, Norway (2006).

Pohorecki, R. M., and Wladyslaw, "Kinetics of Reaction Between Carbon Dioxide and Hydroxyl Ions in Aqueous Electrolyte Solutions," *Chem. Eng. Sci.*, **43**(7), 1677-1684 (1988).

Polderman, L. D., C. P. Dillon, et al., "Why monoethanolamine solution breaks down in gas-treating service," *Oil Gas J.*, **54**(2), 180-183 (1955).

Richardson, B., E. Schussler, and M. Silver, "Regeneration of Monoethanolamine by Gypsum Crystallization for Carbon Capture Systems," ChE 264 special project, University of Texas, Austin (Spring 2006).

Rochelle, G. T., Personal Communication to Andrew Sexton, Austin, TX (2005).

Rochelle, G. T., et al., "CO_2 Capture by Absorption with Potassium Carbonate," Third Quarterly Report, DOE Award #DE-FC26-02NT41440, University of Texas, Austin (2006).

Sachde, D., and S. Sivaram, "CO_2 Capture: Solubility of Potassium Sulfate in Amine Solutions," ChE 264 special project, University of Texas, Austin (Summer 2006)

Shoulders, B., Personal Communication to Andrew Sexton, Austin, TX (2005).

Smith, J. M., H. C. Van Ness, and M. M. Abbott, *Introduction to Chemical Engineering Thermodynamics*, 6th ed., McGraw-Hill, New York (2001).

Smith, P. A. S., and R. N. Loeppky, "Nitrosative Cleavage of Tertiary Amines," *J. ACS*, **89**, 1147-1157 (1967).

Supap, T., R. Idem, et al., "Analysis of Monoethanolamine and its Oxidative Degradation Products during CO_2 Absorption from Flue Gases: A Comparative Study of GC-MS,

HPLC-RID and CE-DAD Analytical Techniques and Possible Optimum Combinations," *Ind. & Eng. Chem. Res.*, **45**(8), 2437-2451 (2006).

Talzi, V. P., "NMR Determination of the Total Composition of Commercial Absorbents Based on Monoethanolamine," *Russian J. App. Chem.*, **77**(3), 437-441 (2004).

Tobiesen, F. A., H. F. Svendsen, and K. A. Hoff, "Desorber energy consumption in amine based absorption plants," *Int. J. Green Energy*, **2**, 1-15 (2005).

Tricker, A. R., R. Kumar, M. Siddiqi, M. S. Khuroo, and R. Preusmann, "Endogenous formation of *N*-nitrosamines from piperazine and their urinary excretion following antihelmintic treatment with piperazine citrate," *Carcinogenesis*, 12**(**9), 1595-1599 (1991).

Wang, J., Personal Communication to Andrew Sexton, Austin, TX (2005).

Weiland, R. H., M. Rawal, and R. G. Rice, "Stripping of carbon dioxide from monoethanolamine solutions in a packed column," *AIChE J.*, **28**(6), 963-973 (1982).

Yazvikova, N. V., L. G. Zelenskaya, et al., "Mechanism of Side Reactions during removal of Carbon Dioxide from Gases by Treatment with Monoethanolamine," *Zhurnal Prikladnoi Khimii*, **48**(3), 674-676 (1975).